

The rp -Process in Neutrino-driven Winds

Shinya Wanajo

Research Center for the Early Universe, Graduate School of Science, University of Tokyo, Bunkyo-ku,
Tokyo 113-0033, Japan; wanajo@resceu.s.u-tokyo.ac.jp

ABSTRACT

Recent hydrodynamic simulations of core-collapse supernovae with accurate neutrino transport suggest that the bulk of the early neutrino-heated ejecta is proton rich, in which the production of some interesting proton-rich nuclei is expected. As suggested in recent nucleosynthesis studies, the rapid proton-capture (rp) process takes place in such proton-rich environments by bypassing the waiting point nuclei with the β^+ -lives of a few minutes via the faster capture of neutrons continuously supplied from the neutrino absorption by protons. In this study, the nucleosynthesis calculations are performed with the wide ranges of the neutrino luminosities and the electron fractions (Y_e), using the semi-analytic models of proto-neutron star winds. The masses of proto-neutron stars are taken to be $1.4 M_\odot$ and $2.0 M_\odot$, where the latter is regarded as the test for somewhat high entropy winds (about a factor of two). For $Y_e > 0.52$, the neutrino-induced rp -process takes place in many wind trajectories, and the p -nuclei up to $A \sim 130$ are synthesized with interesting amounts. However, ^{92}Mo is somewhat underproduced compared to those with similar mass numbers. For $0.46 < Y_e < 0.49$, on the other hand, ^{92}Mo is significantly enhanced by the nuclear flows in the vicinity of the abundant ^{90}Zr that originates from the α -process at higher temperature. The nucleosynthetic yields are averaged over the ejected masses of winds, and further the Y_e distribution predicted by the recent hydrodynamic simulation of a core-collapse supernova. Comparison of the mass- Y_e -averaged yields to the solar compositions implies that the neutrino-driven winds can be potentially the origin of light p -nuclei up to $A \sim 110$, including $^{92,94}\text{Mo}$ and $^{96,98}\text{Ru}$ that cannot be explained by other astrophysical sites.

Subject headings: nuclear reactions, nucleosynthesis, abundances — stars: abundances — stars: neutron — supernovae: general

1. Introduction

The rapid proton-capture (rp) process of nucleosynthesis is expected to take place in proton-rich compositions with sufficiently high temperature (Wallace & Woosley 1981), which leads to the production of proton-rich isotopes beyond iron. This is an analogous phenomenon to the rapid neutron-capture (r) process in neutron-rich compositions, which accounts for the production of about half of the species heavier than iron (see Wanajo & Ishimaru 2006, for a recent review). A major difference between these two processes is the presence of the Coulomb barrier for proton capture reactions. This limits the requisite temperature for this process to a small range, $\sim 1 - 3 \times 10^9$ K, in

which the proton capture proceeds during short time compared to the relevant β^+ -decay lifetimes without substantial photodisintegrations. To date the thermonuclear explosions of hydrogen-rich material on accreting neutron stars (X-ray bursts) have been considered to be the promising astrophysical site associated to the occurrence of rp -process (e.g., Schatz et al. 1998; Koike et al. 1999; Woosley et al. 2004). However, little amount of the nucleosynthetic product is expected to be ejected, whose contribution to the Galactic chemical evolution is likely to be negligible.

Recent hydrodynamic studies of core-collapse supernovae that take the accurate neutrino transport into account have shown that the bulk of the neutrino-heated ejecta during the early phase

($\lesssim 1$ s) is *proton-rich* (Liebendörfer et al. 2003; Buras et al. 2006; Kitaura, Janka, & Hillebrandt 2005; Pruet et al. 2005a; Fröhlich et al. 2006). Given this proton richness in the innermost ejecta is the general characteristic, one might think that core-collapse supernovae provide suitable physical conditions for the *rp*-process. If this is true, the study of *rp*-process in core-collapse supernovae will be of special importance, which no doubt eject the nucleosynthetic products and thus contribute to the Galactic chemical evolution. However, there are a number of nuclei with the β^+ -lives of a few minutes on the *rp*-process path. These “waiting point” nuclei inhibit the production of heavy proton-rich nuclei beyond the iron-group in core-collapse supernovae (Pruet et al. 2005a). The first waiting point nucleus encountered soon after the iron group is ^{64}Ge . The half life of its β^+ -decay is 1.06 min, which is obviously longer than the dynamic timescale of the innermost ejecta of a core-collapse supernova (< 1 s).

The situation changes dramatically, however, when neutrino-induced reactions are included in the nucleosynthesis calculations. In fact, recent studies by Fröhlich et al. (2005, 2006), Pruet et al. (2005b), and Wanajo (2005) have shown that the β^+ -waiting points are bypassed via neutron capture reactions even in proton-rich environments. This is due to the continuous supply of neutrons from the anti-electron neutrino absorption by free protons in the early ejecta that is subject to an intense neutrino flux. As a consequence, the *rp*-process takes place, which leads to the production of proton-rich nuclei beyond the iron group. In particular, the production of some light *p*-nuclei by this neutrino-induced *rp*-process is anticipated in Fröhlich et al. (2005) and Pruet et al. (2005b). In their works, however, only a small number of thermodynamic trajectories were considered for the nucleosynthesis calculations, which were also limited for the very early ejecta ($\lesssim 1$ s after core bounce). This is due to the limitations of the hydrodynamic calculations with accurate neutrino transport currently available, which led to “successful” supernova explosions. It is obvious, however, that more investigations for various physical conditions are needed for a profound understanding of the overall picture of this newly discovered nucleosynthesis process.

In this paper, therefore, the neutrino-induced

rp-process of nucleosynthesis in neutrino-driven winds is investigated in some detail, for various physical conditions obtained from (much simpler) semi-analytic calculations. A special attention is paid for the production of light *p*-nuclei including $^{92,94}\text{Mo}$ and $^{96,98}\text{Ru}$, which cannot be explained even by the most successful scenario (i.e., the O/Ne layers in core-collapse supernovae, Prantzos et al. 1990; Rayet et al. 1995). The production of some light *p*-nuclei (^{74}Se , ^{78}Kr , ^{84}Sr , and ^{92}Mo) in slightly neutron-rich winds has also been suggested by Hoffman et al. (1996). Hence, the nucleosynthesis calculations are performed for the wide range of initial electron fractions (Y_e) covering *both* proton-rich and neutron-rich winds. This is of particular importance to discuss whether the neutrino-driven winds can be the major production site of these light *p*-nuclei.

The thermodynamic and hydrodynamic trajectories of the neutrino-heated ejecta are obtained with the semi-analytic models of neutrino-driven winds (§ 2), which were originally developed for the study of *r*-process (Wanajo et al. 2001). This study is thus a natural extension of the previous nucleosynthesis study in Wanajo et al. (2001), to take the variation of Y_e into consideration (see also Wanajo et al. 2002; Wanajo & Ishimaru 2006). The masses of proto-neutron stars are taken to be $1.4 M_\odot$ and $2.0 M_\odot$ as in Wanajo et al. (2001). The latter is regarded as the test case for (reasonably) high entropy winds (about a factor of two), which has been proposed as a possible model for the production of heavy *r*-nuclei (Otsuki et al. 2000; Wanajo et al. 2001). The nucleosynthesis in each wind trajectory is calculated for the wide range of Y_e including *both* proton-rich and neutron-rich compositions (§ 3). The mass-averaged yields over the various neutrino luminosities for a given initial Y_e are compared with the solar abundances (§ 4). These results are further averaged over the Y_e distribution of the neutrino-heated ejecta obtained from the recent two-dimensional hydrodynamic calculation by Buras et al. (2006). These mass- Y_e -averaged yields are compared to the solar compositions to discuss the contribution of the nucleosynthesis in neutrino-driven winds to the Galactic chemical evolution. Summary and conclusions of the current study are presented in § 5.

2. Neutrino-driven Wind Models

After several 100 ms from the core bounce, hot convective bubbles are evacuated from the surface of a proto-neutron star, and the winds driven by neutrino heating emerge, as can be seen in some hydrodynamic simulations of “successful” supernova explosions (Woosley et al. 1994; Buras et al. 2006). During this wind phase, a steady flow approximation may be justified. The wind trajectories in this paper are thus obtained using the semi-analytic models of neutrino-driven winds in Otsuki et al. (2000) and Wanajo et al. (2001, 2002), which were developed for the study of r -process (see also Qian & Woosley 1996; Cardall & Fuller 1997; Thompson, Burrows, & Meyer 2001). Here the models and some modifications added to them are briefly described.

The system is treated as time stationary and spherically symmetric, and the radius of the neutron star is assumed to be the same as that of the neutrino sphere. The physical variables in the wind are then expressed as functions of the distance r from the center of the neutron star. The ejected mass by neutrino heating is assumed to be negligible compared to the mass of the neutron star. Therefore, the gravitational field in which the neutrino-heated matter moves can be treated as a fixed-background Schwarzschild metric. Time variations of the velocity, temperature, and density can be solved with their boundary conditions by use of relations based on baryon, momentum, and energy conservation (eqs. (1)-(3) in Wanajo et al. 2001). The source term in the equation of energy conservation is due to both heating and cooling by neutrino interactions. The gravitational redshift of the neutrino energies, and the bending of the neutrino trajectories expected from general relativistic effects, are explicitly taken into account (Otsuki et al. 2000). The neutrino luminosities L_ν of all neutrino flavors are assumed to be equal, and the rms average neutrino energies are taken to be 10, 20, and 30 MeV, for electron, anti-electron, and the other flavors of neutrinos, respectively.

As the boundary conditions at the neutrino sphere, the density is taken to be $10^{10} \text{ g cm}^{-3}$ and the temperature is determined so that heating and cooling by neutrino interactions are in equilibrium. The mass ejection rate at the neutrino sphere \dot{M}

that determines the initial velocity is set to be $\dot{M} = 0.99 \times \dot{M}_c$. Here \dot{M}_c is the critical value that gives the transonic solution. The wind with \dot{M}_c becomes supersonic through the sonic point, while those with $\dot{M} < \dot{M}_c$ are subsonic throughout. In fact, recent hydrodynamic simulations show that the fast wind collides with the dense shell of slower ejecta behind the shock and is decelerated again to be subsonic (e.g., Buras et al. 2006). On the other hand, the subsonic wind, which cannot escape by itself from the gravitational potential, must be enough fast (i.e., $\dot{M} \approx \dot{M}_c$) to reach the early *bubble* ejecta. For example, the wind is too slow to reach the ejecta behind the shock (at several 1000 km) when \dot{M} is taken to be $0.9 \times \dot{M}_c$. Thus, the choice of \dot{M} above may be reasonable.

In this study, the neutron star masses M are taken to be $1.4 M_\odot$ and $2.0 M_\odot$. The radius of neutrino sphere is assumed to be $R_\nu(L_\nu) = (R_{\nu 0} - R_{\nu f})(L_\nu/L_{\nu 0}) + R_{\nu f}$ as a function of L_ν , where $R_{\nu 0} = 30 \text{ km}$, $R_{\nu f} = 10 \text{ km}$, and $L_{\nu 0} = 4 \times 10^{52} \text{ ergs s}^{-1}$, as shown in Figure 1 (*dashed line*). This mimics the early time evolution of neutrino sphere that can be seen in realistic core-collapse simulations (Woosley et al. 1994; Buras et al. 2006, see also Figures 2 and 3). In Figure 1, \dot{M} for each M is also shown as a function of L_ν (*solid line*). The resulted (asymptotic) entropy per baryon s and the dynamic timescale $\tau_{\text{dyn}} (\equiv |\rho/(d\rho/dt)|_{T=0.5 \text{ MeV}})$ are denoted by thick solid and dot dashed lines, respectively. As can be seen, the model of $M = 2.0 M_\odot$ results in higher s , shorter τ_{dyn} , and smaller \dot{M} . In particular, the entropy is as twice as that for the $M = 1.4 M_\odot$ model all the way, which might lead to the production of the heavy r -process nuclei (Otsuki et al. 2000; Wanajo et al. 2001).

It should be noted that no hydrodynamic studies to date indicate the formation of such a massive proto-neutron star (with the radius of $\sim 10 \text{ km}$). On the other hand, a recent hydrodynamic simulation shows an entropy increase owing to the collision with the slower preceding ejecta, resulting $s \sim 80 N_A k$ at early times ($\sim 1 \text{ s}$, Pruet et al. 2005a; Buras et al. 2006). Furthermore, some other mechanisms that increase entropy have been also proposed (e.g., Qian & Woosley 1996; Thompson 2003; Suzuki & Nagataki 2005; Burrows et al. 2005). In fact, when it comes to merely entropy, the model of $M = 2.0 M_\odot$ is rather close to the

hydrodynamic implication in Pruet et al. (2005a) as far as during the early epoch. Thus, this model can be regarded simply as a *reasonably* high entropy case that would be expected in realistic simulations, rather than an extreme case with a very massive proto-neutron star. This may be better than to obtain the higher entropy by multiplying a certain factor to the density or temperature with no physical basis. It should be stressed that the time variations of the temperature, density, and distance from the center of the neutron star are obtained consistently in the current study, which are all important for the nucleosynthesis (§ 3.3).

In order to link the current time stationary solutions to more realistic, time-evolving neutrino-driven winds, the evolution of L_ν is assumed to be $L_\nu(t_{\text{pb}}) = L_{\nu 0}(t_{\text{pb}}/t_0)^{-1}$ as a function of the post bounce time t_{pb} (Figure 1, *dotted line*), where $t_0 = 0.2$ s. This approximately mimics the hydrodynamic results of the neutrino-driven winds in Woosley et al. (1994). This gives the time evolution of the neutrino sphere to be $R_\nu(t_{\text{pb}}) = (R_{\nu 0} - R_{\nu f})(t_{\text{pb}}/t_0)^{-1} + R_{\nu f}$ (Figs. 2 and 3). The wind trajectories are calculated for 54 constant L_ν of $40 - 0.5 \times 10^{51}$ ergs s^{-1} ($0.2 \leq t_{\text{pb}} \leq 16$ s) with the intervals of 1×10^{51} ergs s^{-1} and 1×10^{50} ergs s^{-1} for $L_\nu \geq 2 \times 10^{51}$ ergs s^{-1} ($t_{\text{pb}} \leq 4$ s) and $L_\nu < 2 \times 10^{51}$ ergs s^{-1} ($t_{\text{pb}} > 4$ s), respectively.

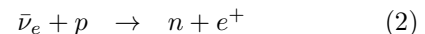
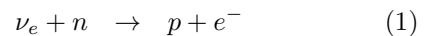
The time evolutions of r , T_9 ($\equiv T/10^9$ K), ρ , and s for selected (odd-numbered) trajectories are shown in Figures 2 (for $M = 1.4 M_\odot$) and 3 (for $M = 2.0 M_\odot$). As can be seen in the top panels of these figures, the time evolutions of radii for $t_{\text{pb}} > 0.5$ s are very similar to those found in the hydrodynamic results (Woosley et al. 1994; Buras et al. 2006), at which the current wind solutions may be justified. On the other hand, the early time evolutions for $t_{\text{pb}} < 0.5$ s seem less realistic, in which the convective bubbles dominate in a realistic simulation (Buras et al. 2006). This may not cause a severe problem, since the rp -process takes place dominantly at $t_{\text{pb}} > 0.5$ s as discussed in § 3.3. Both models ($M = 1.4 M_\odot$ and $2.0 M_\odot$) show qualitatively similar thermodynamic histories as can be seen in Figures 2 and 3. Note, however, that the entropy is about a factor of two higher for the $M = 2.0 M_\odot$ model all the way.

3. Nucleosynthesis in Winds

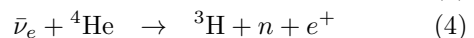
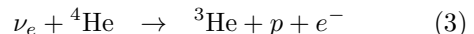
3.1. Reaction Network

Adopting the wind trajectories discussed in § 2 for the physical conditions, the nucleosynthetic yields are obtained by solving an extensive nuclear reaction network code. The network consists of 6300 species between the proton and neutron drip lines predicted by a recent fully microscopic mass formula (HFB-9, Goriely et al. 2005), all the way from single neutrons and protons up to the $Z = 110$ isotopes. All relevant reactions, i.e. (n, γ) , (p, γ) , (α, γ) , (p, n) , (α, n) , (α, p) , and their inverse are included. The experimental data whenever available and the theoretical predictions for light nuclei ($Z < 10$) are taken from the REA-CLIB compilation (F. -K. Thielemann 1995, private communication). All other reaction rates are taken from the Hauser-Feshbach rates of BRUSLUB (Aikawa et al. 2005) making use of experimental masses (Audi, Wapstra, & Thibault 2003) whenever available or the HFB-9 mass predictions (Goriely et al. 2005) otherwise. The photodisintegration rates are deduced applying the reciprocity theorem with the nuclear masses considered. The β -decay rates are taken from the gross theory predictions (GT2, Tachibana, Yamada, & Yoshida 1990), obtained with the HFB-9 Q_β predictions (T. Tachibana 2005, private communication). Electron capture reactions on free nucleons as well as on heavy nuclei are also included (Fuller, Fowler, & Newman 1982; Langanke & Martinez-Pinedo 2001).

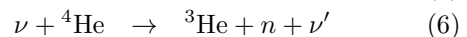
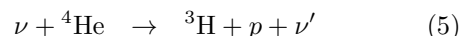
Rates for neutrino capture on free nucleons



and ${}^4\text{He}$,



as well as for neutrino spallation of free nucleons from ${}^4\text{He}$,



are also included (Woosley et al. 1990; McLaughlin, Fuller, & Wilson 1996). Neutrino-induced reactions of heavy nuclei are not included in this

study, which may have only minor effects (Meyer, McLaughlin, & Fuller 1998). The rates for neutrino reactions above are expressed as (Qian et al. 1997)

$$\lambda_\nu \approx 4.97 \left(\frac{L_\nu}{10^{51} \text{ ergs s}^{-1}} \right) \left(\frac{\text{MeV}}{\langle E_\nu \rangle} \right) \times \left(\frac{100 \text{ km}}{r} \right)^2 \left(\frac{\langle \sigma_\nu \rangle}{10^{-41} \text{ cm}^2} \right) \text{ s}^{-1}, \quad (7)$$

where $\langle E_\nu \rangle$ and $\langle \sigma_\nu \rangle$ are the average energy and cross section of the neutrino species responsible for the reaction. The time evolution of L_ν is taken into account, according to $L_\nu(t_{\text{pb}})$ in § 2. The distance r from the center of the neutron star for each wind as a function of time can be seen in Figures 2 and 3.

3.2. Initial Compositions and Y_e

Each calculation is initiated ($t = 0$ s) when the temperature decreases to $T_9 = 9$ (where $T_9 \equiv T/10^9$ K). At this high temperature, the compositions in the nuclear statistical equilibrium (NSE) are obtained (mostly free nucleons and α particles) immediately after the calculation starts. The initial compositions are thus given by $X_n = 1 - Y_{ei}$ and $X_p = Y_{ei}$, respectively, where X_n and X_p are the mass fractions of neutrons and protons, and Y_{ei} is the initial electron fraction (number of proton per nucleon) at $T_9 = 9$. In a core-collapse simulation for long duration (~ 20 s, Woosley et al. 1994), it is observed that the initial Y_e takes mostly a constant value (≈ 0.46) during the early phase ($t_{\text{pb}} =$ a few s), and gradually decreases to ≈ 0.36 . This is due to the hardening of the anti-electron neutrino spectrum relative to that of the electron neutrino at later times (Qian & Woosley 1996). In order to mimic this effect, Y_{ei} is assumed to be constant (Y_{e0}) for $t_0 < t \leq t_1$ and $Y_e(t) = (Y_{e0} - Y_{ef})(t/t_1)^{-1} + Y_{ef}$ for $t > t_1$, where $t_1 = 4$ s and $Y_{ef} = 0.1$. This gives Y_{ei} for each wind such as $Y_e = Y_{e0}$ and $Y_e(L_\nu) = (Y_{e0} - Y_{ef})(L_\nu/L_{\nu 0})(t_1/t_0) + Y_{ef}$ for $L_\nu \geq 2 \times 10^{51}$ ergs s $^{-1}$ and $L_\nu < 2 \times 10^{51}$ ergs s $^{-1}$, respectively.

The core-collapse simulation in Woosley et al. (1994) shows that the neutrino-heated ejecta at the first few seconds is *neutron rich* ($Y_e \approx 0.46$). On the other hand, recent hydrodynamic studies with more accurate neutrino transport show that

the bulk of the ejecta during the early phase is *proton rich* ($Y_e \gtrsim 0.5$, Liebendörfer et al. 2003; Kitaura, Janka, & Hillebrandt 2005; Buras et al. 2006). The reason of this proton richness is that, when the degeneracy is lifted, the mass difference between the proton and neutron favors the proton-rich composition as far as the differences of luminosities and mean energies between the electron neutrinos and the anti-electron neutrinos are not significant. As a result, the electron neutrino capture (eq. [1]) and the positron capture (inverse of eq. [2]) overcome their inverses, resulting in $Y_e > 0.5$ (see Hoffman et al. 1996; Fröhlich et al. 2006; Buras et al. 2006, for more detailed discussion). In this study, the nucleosynthesis calculation for each wind is repeated for various Y_{e0} ($= 0.45\text{--}0.65$) with the interval of 0.005 (41 cases), covering the slightly neutron-rich to very proton-rich compositions. In Figure 4 (*top panel*), the time variations of Y_{ei} that determines the initial composition for each wind are shown for the winds of $M = 2.0 M_\odot$ with $Y_{e0} = 0.60$ (*thin solid line*) and $M = 1.4 M_\odot$ with $Y_{e0} = 0.48$ (*thin dotted line*), respectively.

Neutrino capture on free nucleons changes Y_e (“ α effect”, McLaughlin, Fuller, & Wilson 1996; Meyer, McLaughlin, & Fuller 1998). Figure 5 shows Y_e (*thick lines*) along with the mass fractions (*thin lines*) of neutrons X_n , protons X_p , α particles X_α , and heavy nuclei X_h ($Z > 2$) as functions of T_9 , obtained from nucleosynthesis calculations for the winds with $M = 2.0 M_\odot$, $L_\nu = 1 \times 10^{52}$ ergs s $^{-1}$, and $Y_{e0} = 0.60$ (W201060, *solid lines*) and $M = 1.4 M_\odot$, $L_\nu = 1 \times 10^{52}$ ergs s $^{-1}$, and $Y_{e0} = 0.48$ (W141048, *dotted lines*), respectively¹. For the wind W201060, Y_e decreases significantly as the temperature drops. This is due to the increasing α particles, which continues as far as neutrons are supplied from the neutrino capture on protons (eq. [2]). The electron fraction can be expressed as

$$Y_e \approx X_p + \frac{X_\alpha}{2} + \sum_{Z>2,A} ZY(Z,A), \quad (8)$$

where $Y(Z, A)$ is the abundance (number fraction per nucleon, i.e., the mass fraction divided by A) of

¹The wind trajectory with $M = i.j M_\odot$, $L_\nu = kl \times 10^{51}$ ergs s $^{-1}$, and $Y_{e0} = 0.mn$ is labeled as *Wijklmn*, hereafter.

the nucleus (Z, A). For W201060, alpha particles dominate with a small fraction of protons as soon as the temperature drops to $T_9 \sim 7$. Hence the second term of equation (8) governs Y_e , while the third term is negligible. As a result, Y_e decreases toward 0.5. Note that the decrease of Y_e for $T_9 \lesssim 3$ is due to the (n, p) reactions during the rp -process phase and the β^+ -decays after freezeout (§ 3.3). On the other hand, for W141048, α particles and also heavy nuclei dominate at $T_9 \sim 6$. Thus, Y_e is determined by the second and third terms in equation (8). The sum of these two terms are close to the original Y_e value ($= 0.48$), owing to the slight neutron richness of heavy nuclei. As a result, Y_e keeps its original value.

This can be seen in Figure 4 (*bottom panel*), in which the changes of Y_e , ΔY_e , until the temperature drops to $T_9 = 3$ (at which the rp -process begins, see § 3.3) as function of Y_{e0} , for the winds with $M = 1.4 M_\odot$ (*dotted line*) and $2.0 M_\odot$ (*solid line*). The change is not significant for $Y_{e0} \approx 0.47 - 0.48$ as described above. For a larger Y_{e0} case (> 0.5), $|\Delta Y_e|$ is greater for the more massive $M (= 2.0 M_\odot)$ model at later times ($t_{\text{pb}} = 4$, i.e., $L_\nu = 2 \times 10^{51}$ ergs s^{-1}). This is due to the greater entropy for these winds (see Figures 1-3) that leave more free protons for $Y_e > 0.5$. For the same reason, $|\Delta Y_e|$ is also greater for a larger Y_{e0} case. For a smaller Y_{e0} case ($\lesssim 0.47$), ΔY_e takes a positive value owing to the abundant neutrons. The electron fraction at $T_9 = 3$, defined as $Y_{ef} \equiv Y_{ei} + \Delta Y_e$, is shown as a function of t_{pb} in Figure 4 (*top panel, thick lines*) for the winds of $M = 2.0 M_\odot$ with $Y_{e0} = 0.60$ (*solid line*) and $M = 1.4 M_\odot$ with $Y_{e0} = 0.45$ (*dotted line*). At later times ($t_{\text{pb}} > 4$ s), in which the material is assumed to be rather neutron rich, Y_e increases significantly owing to the neutrino effect and takes $\approx 0.34 - 0.36$ at $t_{\text{pb}} = 16$ s ($L_\nu = 5 \times 10^{50}$ ergs s^{-1}). Note that the time evolution of Y_{ef} for $M = 1.4 M_\odot$ with $Y_{e0} = 0.45$ (Fig. 4, *top panel, thick dotted line*) is similar to the hydrodynamic result in Woosley et al. (1994).

3.3. The rp -Process in Proton-rich Winds

In the proton-rich compositions with the presence of intense neutrino flux, the proton capture proceeds beyond the iron group nuclei by bypassing the β^+ -waiting point nuclei, as shown in recent works (Fröhlich et al. 2005, 2006; Pruet et al. 2005a; Wanajo 2005). This can be clearly

seen in Figure 6, which compares the snapshots of nucleosynthesis at $t = 0.22$ s (when the temperature drops to $T_9 \approx 2$) for W141060 without (*left panel*) and with (*right panel*) neutrino reactions. Without neutrino reactions, the nuclear flow cannot advance beyond ^{64}Ge , whose β^+ half life is 1.06 minutes². In contrast, the neutrino capture on abundant protons (eq. [2]) provides a fraction of neutrons that immediately suffer (n, p) reactions. Note that the (n, p) reaction acts as the same as the β^+ -decay of a given species. As a result, the nuclear flow proceeds to the heavier proton-rich species (Fig. 6, *right panel*).

It is interesting to note that the proton-to-seed abundance ratio Y_p/Y_h at this point (Figure 6, *right panel*) is still high ($= 49$) despite the moderate entropy ($55 N_A k$). This is due to the slowness of the $\alpha + \alpha + \alpha \rightarrow ^{12}\text{C}$ reaction that is the bottleneck for the production of heavy nuclei. This is in contrast to the neutron-rich compositions, in which the faster $\alpha + \alpha + n \rightarrow ^9\text{Be}$ reaction followed by α capture is efficient. This is why the entropy of a few $100 N_A k$ is needed for the r -process in neutrino-driven winds (Woosley et al. 1994; Wanajo et al. 2001). In the proton-rich compositions, however, only a moderate entropy is sufficient for the occurrence of rp -process.

This *neutrino-induced* rp -process can be seen more clearly for the wind models with $M = 2.0 M_\odot$. This is a consequence of their higher entropies (see Figures 1-3), which leave more protons needed for the rp -process. Figure 7 shows the snapshots of nucleosynthesis calculations for the winds W201060 (*top panels*), W200865 (*middle panels*), and W200265 (*bottom panels*) during ($T_9 \approx 2$, *left panels*) and after ($t \approx 1.0$ s, *right panels*) the rp -process phase. For the same L_ν and Y_{e0} to W141060 (Fig. 6, *right panel*) but with $M = 2.0 M_\odot$ (W201060), Y_p/Y_h is three times greater ($= 151$) at $T_9 = 2$ (Fig. 7, *top left*), owing to its higher entropy ($= 92 N_A k$). As a result, the nuclear flow proceeds to the $Z = 50$ magic nuclei, which leads to the production of the p -nuclei with

²In the current reaction network, ^{65}As is omitted, whose proton separation energy is predicted to be negative in the HFB-9 mass formula (Goriely et al. 2005). Inclusion of this isotope would not change the current result, however, since the proton separation energy of this nucleus was estimated be no more than 0.2 MeV (Audi, Wapstra, & Thibault 2003; Pruet et al. 2005b).

$A \sim 110$.

The detailed nuclear flow patterns for W201060 when the rp -process is active ($T_9 = 2.5$) are shown in Figure 8. Here, the nuclear flow for each reaction $i \rightarrow j$ is defined as

$$F_{ij} \equiv \dot{Y}(i \rightarrow j) - \dot{Y}(j \rightarrow i) \quad \text{s}^{-1}. \quad (9)$$

In Figure 8, F_{ij} and Y_i (for those greater than 10^{-5}) are shown in logarithmic scale by arrows and circles, respectively. As can be seen, (p, n) reactions play a dominant role to carry away the nuclear abundances from waiting points, while the contribution of β^+ -decays (off-centered arrows) is minor.

The time variations of the mass fractions (*thin lines*) of neutrons X_n , protons X_p , α particles X_α , and heavy nuclei X_h for W201060 are shown in Figure 9, along with those of the average mass number of heavy nuclei A_h and the temperature (*thick lines*), where

$$X_h \equiv \sum_{Z>2,A} X(Z, A) \quad (10)$$

and

$$A_h \equiv \frac{1}{X_h} \sum_{Z>2,A} A X(Z, A). \quad (11)$$

The results with all neutrino-induced reactions (eqs. [1]-[6]), neutrino capture on free nucleons only (eqs. [1] and [2]), and no neutrino-induced reactions are denoted by the solid, dashed, and dotted lines, respectively. The initiation of the rp -process can be clearly seen as the sudden increase of A_h at $T_9 \approx 3$, for the cases with neutrino reactions (*thick solid* and *thick dashed lines*). This is due to the presence of neutrons ($X_n \sim 10^{-11}$) by the neutrino capture on abundant protons (eq. [2]), as can be seen in Figure 9 (*thin solid* and *thin dashed lines*).

The neutrino reactions for ${}^4\text{He}$ tend to inhibit the rp -process as can be seen in Figure 9, although their effects are moderate. This is due to the spallation reactions of ${}^4\text{He}$ (eqs. [5] and [6]), while the capture reactions (eqs. [3] and [4]) are not important (because of their smaller cross sections). The resulting ${}^3\text{H}$ emitted from the neutrino spallation of equation (5) immediately suffers a (p, n) reaction to ${}^3\text{He}$ in the proton-rich compositions. These ${}^3\text{He}$ nuclei, in addition to those from the spallation

reaction of equation (6), capture abundant α particles to be ${}^7\text{Be}$, which further capture α particles. As a result, a fraction of ${}^4\text{He}$ assembles into heavier nuclei that act as “neutron poison”, resulting in the smaller neutron abundance (Figure 9). This is a similar mechanism shown by Meyer (1995), i.e., the r -process is also inhibited by these neutrino reactions on ${}^4\text{He}$ in the neutron-rich compositions. It should be noted that the relatively large mean energies of μ and τ neutrinos assumed in this study (according to Woosley et al. (1994)) may lead to the overestimation of this effect.

In order to see the gross feature of the neutrino-induced rp -process more clearly, the time variations of the mean lifetimes for β^+ -decay, (n, γ) , (p, γ) , and (n, p) reactions, and neutrino capture on protons (eq. [2]) are shown in Figure 10 (*solid lines*), where

$$\tau_{\beta^+} \equiv \left[\frac{1}{Y_h} \sum_{Z>2,A} \lambda_{\beta^+}(Z, A) Y(Z, A) \right]^{-1}, \quad (12)$$

$$\tau_{n\gamma} \equiv \left[\frac{\rho Y_n}{Y_h} \sum_{Z>2,A} \lambda_{n\gamma}(Z, A) Y(Z, A) \right]^{-1}, \quad (13)$$

$$\tau_{p\gamma} \equiv \left[\frac{\rho Y_p}{Y_h} \sum_{Z>2,A} \lambda_{p\gamma}(Z, A) Y(Z, A) \right]^{-1}, \quad (14)$$

$$\tau_{np} \equiv \left[\frac{\rho Y_n}{Y_h} \sum_{Z>2,A} \lambda_{np}(Z, A) Y(Z, A) \right]^{-1}, \quad (15)$$

and

$$\tau_{\bar{\nu}_e p} \equiv \lambda_{\bar{\nu}_e p}^{-1}. \quad (16)$$

Here,

$$Y_h \equiv \sum_{Z>2,A} Y(Z, A) \quad (17)$$

and $\lambda_{\beta^+}(Z, A)$, $\lambda_{n\gamma}(Z, A)$, $\lambda_{p\gamma}(Z, A)$, $\lambda_{np}(Z, A)$, and $\lambda_{\bar{\nu}_e p}$ are the rates of the corresponding reactions. The rates in equations (12)-(15) are averaged over the heavy nuclei, which represent the lifetimes of the dominant isotopes at a given time. The dotted lines are the corresponding lifetimes when the sum in equations (12)-(15) are taken for $Z \geq 48$ only. With the timescales defined above, the requisite condition for the neutrino-induced rp -process can be expressed as

$$\tau_{p\gamma} \ll \tau_{np} \ll \tau_{\beta^+}. \quad (18)$$

Note that the conditions for the r -process and classical rp -process are simply $\tau_{n\gamma} \ll \tau_{\beta^-}$ and $\tau_{p\gamma} \ll \tau_{\beta^+}$, respectively.

Top panel of Figure 10 is the result for the wind trajectory of W201060 that is taken to be the reference case here. As can be seen, the (n, p) reactions are faster than the β^+ -decays all the way during the first one second. This shows clearly the importance of the (n, p) reactions for the neutrino-induced rp -process. The role of (n, γ) reactions is minor, compared to (n, p) reactions. A saturation of A_h at $t =$ a few 100 ms ($T_9 \sim 2$) in Figure 9 indicates the termination of the neutrino-induced rp -process. At later times, A_h slightly decreases by photodisintegration. Note that this termination is *not* due to the exhaustion of protons, as in the case of r -process that ceases generally by the neutron exhaustion (Wanajo et al. 2004). The proton-to-seed abundance ratio is still high at later times (e.g., $Y_p/Y_h = 77$ at $t = 1$ s), and the bulk of (p, γ) reactions are enough fast throughout (Fig. 10, *solid line*). However, the (p, γ) reactions for the heaviest nuclei ($Z \geq 48$; Fig. 10, *dotted line*) become slow owing to the increasing Coulomb barrier, and compete with the (n, p) reactions (i.e., $\tau_{p\gamma} \sim \tau_{np}$) at $t \sim 0.1$ s ($T_9 \sim 2$). This results in the broadening and smoothing of the abundances for $Z > 40$ in Figure 7 (*top panels*), which is similar to the “freezeout effect” seen in the r -process (Wanajo et al. 2004).

What terminates the rp -process is thus the Coulomb barrier of the heaviest nuclei in the nuclear flow, which breaks the relation between the first two in equation (18). The slowness of the (n, p) reactions that compete with the β^+ -decays ($\tau_{np} \sim \tau_{\beta^+}$) can be another reason to cease the rp -process. The (n, p) reactions becomes significantly slow owing to the less active neutrino capture on protons (Figure 10) at later times ($t \gtrsim 1$ s), whose lifetime is proportional to the square of r (eqs. [7] and [16]). For the current wind trajectory (W201060), the relation between the latter two in equation (18) breaks only at late times ($t \approx 1$ s for $Z \geq 2$ and $t \approx 7$ s for $Z \geq 48$). This shows that the supply of neutrons by the neutrino capture on protons is sufficient throughout the rp -process phase.

One may consider that the neutrino-induced rp -process proceeds to much higher atomic number to produce *all* the p -nuclei up to $A \sim 200$, *if* the pro-

ton concentration is much higher owing to, e.g., a larger Y_{e0} or a higher entropy. This may not be true, however, as can be seen in Figure 7. For the wind trajectory with a larger entropy ($= 103 N_{Ak}$) and $Y_{e0} (= 0.65, W200865)$ that results in $Y_{ef} = 0.582$, $Y_p/Y_h = 427$ at $T_9 = 2$ and the nuclear flow proceeds beyond $Z = 50$ (Figure 7, *middle panels*). In fact, this wind results in the production of the heaviest p -nuclei with $A \sim 130$. However, the flow deviates from the proton-drip line and reaches the β -stability line (Figure 7, *middle right*, see also Pruet et al. 2005b). This is *not* due to the β^+ -decays of the heaviest nuclei, which are rather slow all the way ($\tau_{\beta^+} \sim 100$ s for $Z \geq 48$; Fig. 10, *middle panel, dotted line*). This is a consequence of the higher and higher Coulomb barrier for the heaviest nuclei in the flow, which competes with both (n, p) and (n, γ) reactions as can be seen in Figure 10 (*middle panel, dotted lines*). In addition, the proton capture slows substantially when the temperature drops below $T_9 \sim 2$ (Figure 10). Thus, the temperature range in which the neutrino-induced rp -process takes place is strictly limited to $2 \lesssim T_9 \lesssim 3$. This differs significantly from the neutron capture without Coulomb barrier in case of the r -process.

At the later wind phase, the entropy increases significantly, as can be seen in Figures 1-3. The situation is even worse (but interesting), however, for the production of proton-rich nuclei. The snapshots of the nucleosynthesis calculations for the wind trajectory of W200265 is shown in Figure 7 (*bottom panels*). This wind obtains the highest entropy ($= 176 N_{Ak}$) during the proton-rich phase assumed in this study ($t_{pb} \leq 4$ s, see Fig. 4, *top panel*). As can be seen, the nuclear flow cannot sustain its proton richness and runs toward the β -stability when the temperature drops to $T_9 \approx 2$ (Figure 7, *bottom left*) despite its extremely high $Y_p/Y_h (= 858)$. At later times, the (n, γ) reactions push the flow to the neutron-rich side (Figure 7, *bottom right*). The reason is that the temperature falls off to $T_9 \approx 1$ quickly in the later winds (Figure 3). As can be seen in Figure 10 (*bottom panel*), when the temperature is below $T_9 \sim 2$, the (p, γ) reactions for the heaviest nuclei in the flow become significantly slow, while the (n, γ) reactions are still active. As can be seen in these examples, the neutrino-induced rp -process may not lead to the significant production of p -nuclei be-

yond $A \sim 130$. It is interesting to note that many of the nuclei synthesized here (Fig. 7, *bottom right panel*) are usually assigned as s -nuclei or even r -nuclei, which are now synthesized in *proton-rich* compositions (see also Pruet et al. 2005b).

3.4. ^{92}Mo Production in Slightly Neutron-rich Winds

In slightly neutron-rich compositions ($Y_e \approx 0.47 - 0.49$), two dominant quasi-statistical-equilibrium (QSE) clusters are formed around $A \approx 60$ and $A \approx 90$ during the α -process phase ($T_9 \approx 7 - 4$). At the end of the α -process phase, the matter consists of mostly α particles, the heavy nuclei belong to these two QSE clusters, and a fraction of free nucleons (Figure 12). As soon as the α -process ceases, the proton capture plays an important role for the production of the p -isotope ^{92}Mo as suggested by Hoffman et al. (1996), whose origin has been a long-standing mystery (see Arnould & Goriely 2003, for a recent review). The nucleosynthesis calculations covering the slightly neutron-rich winds are thus needed to estimate their possible contribution to the Galactic chemical evolution of the light p -nuclei.

As shown in Figure 11, a fraction of the most dominant species ^{90}Zr ($N = 50, Z = 40$) in the QSE cluster (at $A \sim 90$) flows into ^{92}Mo ($N = 50, Z = 42$) through various nuclear channels. The abundance of ^{92}Mo reaches 17% of its final value at this time ($T_9 = 3.5$). Here, the (p, n) reaction plays a dominant role to carry away the nuclear abundances from ^{90}Zr . In Figure 12, the time variations of the mass fractions (*thin lines*) of neutrons X_n , protons X_p , α particles X_α , heavy nuclei X_h , ^{90}Zr , and ^{92}Mo for the wind trajectory of W141048 are shown, along with those of the average mass number of heavy nuclei (A_h , eq. [11]) and the temperature (*thick lines*). Note that the neutrino effect on Y_e is negligible for this wind as described in § 3.1, i.e., $Y_{ef} \approx Y_{e0} = 0.48$. The decrease of X_p slows as the QSE cluster that contains ^{90}Zr grows (at $T_9 \approx 5$), in order to balance with the electron fraction of the cluster (≈ 0.44) that is smaller than that of the wind material (≈ 0.48). These protons are gradually absorbed by the nuclei in this cluster after the α -process phase. As a result, the abundance of ^{92}Mo increases, reaching its half final value at $T_9 = 3.2$.

The enhancement of ^{92}Mo in this way is highly

dependent on the temperature history of the wind after the α -process phase. The production of ^{92}Mo relies largely upon the slower (p, n) reactions (mean lifetime of about 30 ms at $T_9 = 3.5$) on ^{90}Zr , since the photodisintegration impedes the much faster (p, γ) reaction at this time (Figure 11). Another channel, that is the (n, γ) reaction on ^{90}Zr , also contributes but suffers from its inverse. The (p, γ) reaction on ^{90}Zr becomes effective only when the temperature drops below $T_9 \approx 2.7$ for W141048. Therefore, a relatively long cooling timescale of the wind material is required to obtain a large abundance of ^{92}Mo (that is close to its QSE value, see Hoffman et al. 1996). In the current study, the subsonic solutions of winds with $\dot{M} \approx \dot{M}_c$ are adopted as discussed in § 2. As a result, the wind is decelerated when passing over the sonic radius, and thus the decrease of temperature slows down. For the early winds ($t_{\text{pb}} < 1$ s), this transition takes place around $T_9 \approx 4 - 3$. As a result, ^{90}Zr suffers (p, n) and (n, γ) reactions for longer duration, resulting in the more production of ^{92}Mo . Other light p -nuclei, e.g., ^{94}Mo and $^{96,98}\text{Ru}$, are not significantly produced in this process, although ^{74}Se and ^{78}Kr are moderately enhanced (see § 4, see also Hoffman et al. 1996).

It should be noted that the flow patterns appeared in Figure 11 would be somewhat different when another nuclear data set were adopted. In fact, most of the relevant reactions here are taken from the theoretical (Hauser-Feshbach) predictions, although these nuclear masses are well determined by experiments (Audi, Wapstra, & Thibault 2003). Future determinations of these rates based on experiments are highly desirable.

Neutrino-induced reactions are not of importance for the production of ^{92}Mo in these neutron-rich winds. The results with all neutrino-induced reactions (eqs. [1]-[6]), free nucleons only (eqs. [1] and [2]), and no neutrino-induced reactions are denoted by the solid, dashed, and dotted lines, respectively. The dashed and dotted lines cannot be distinguished, which means that the neutrino capture on free nucleons plays no role. This is due to their small abundances as can be seen in Figure 12. The neutrino capture on ^4He does not play a significant role, either. The spallation of free nucleons from ^4He , on the other hand, slightly enhances the abundance of ^{92}Mo . The ^3H and ^3He nuclei emitted from the spallation reactions (eqs. [5] and

[6]) immediately capture abundant α particles to be ${}^7\text{Be}$ and ${}^7\text{Li}$, which further capture α particles. The spalled free nucleons can survive owing to the faster α capture, resulting in the slight increase of ${}^{92}\text{Mo}$ as can be seen in Figure 12.

3.5. The r -Process in Neutron-rich Winds

At later times ($t_{\text{pb}} > 4\text{ s}$), the entropy of the winds increases more than $100 N_A k$ (Figs. 1-3), and Y_{ei} is assumed to be neutron rich (Fig. 4, *top panel*). This may provide the suitable condition for the production of r -process nuclei (Woosley et al. 1994; Wanajo et al. 2001). As discussed in § 4, the winds with $M = 1.4 M_\odot$ can be the origin of only the light r -process nuclei (up to $A \sim 130$; Fig. 15, *top panel*). On the other hand, the heavy r -process nuclei (up to $A \sim 190$) can be produced in the winds with $M = 2.0 M_\odot$ during the late phase (Fig. 15, *bottom panel*). This is a consequence of the higher entropies (Figs. 1-3) and in part the shorter dynamic timescales (Fig. 1) of the winds, resulting in the higher neutron-to-seed abundance ratios at the beginning of r -processing ($T_9 \sim 3$, see Wanajo et al. 2001; Wanajo & Ishimaru 2006, for more detail). Note that the nucleosynthetic results in the later winds do not contribute to the production of proton-rich isotopes (§ 4), since Y_{ei} is assumed to quickly drop to be rather neutron rich (Figure 4, *top panel*).

4. Contribution to the Galactic Chemical Evolution

4.1. Mass-averaged Yields as Functions of Y_e

In order to estimate the contribution of the neutrino-induced rp -process in neutrino-driven winds to the Galactic chemical evolution, the nucleosynthetic yields for each Y_{ei} model (41 cases) are mass-averaged over the 54 wind trajectories weighted by $\dot{M}(L_\nu)\Delta t_{\text{pb}}$. Figure 13 compares the averaged mass fractions X_{ej} of p -nuclei with respect to their solar values (Anders & Grevesse 1989) as functions of Y_{ef} for $M = 1.4 M_\odot$ (*top left*) and $2.0 M_\odot$ (*top right*) models. Here, Y_{ef} , which is approximately the value at the beginning of the rp -process phase (at $T_9 = 3$, § 3.3), is taken at $t_{\text{pb}} = 4\text{ s}$ (at $L_\nu = 2 \times 10^{51}\text{ ergs s}^{-1}$) as representative of different Y_{ef} . The abundances of ${}^{64}\text{Zn}$ and ${}^{90}\text{Zr}$ are also plotted for comparison

purposes. The contribution of p -nuclei produced during the later phase ($t > 4\text{ s}$) is not important, as discussed in § 4.2. Figure 13 also shows the results for selected winds (not mass-averaged) for $L_\nu = 8 \times 10^{51}\text{ ergs s}^{-1}$ ($t_{\text{pb}} = 1\text{ s}$, *middle panels*) and $L_\nu = 2 \times 10^{51}\text{ ergs s}^{-1}$ ($t_{\text{pb}} = 4\text{ s}$, *bottom panels*). The histogram that is taken from Buras et al. (2006) is the asymptotic Y_e distribution $p(Y_e)$ of the neutrino-processed ejecta during the first 468 ms after core bounce for a $15 M_\odot$ progenitor star, obtained by their two-dimensional hydrodynamic simulation.

As can be seen, a variety of p -nuclei are produced with interesting amounts for $Y_{ef} > 0.5$ models. The heavier p -nuclei (up to $A \sim 130$) appear for the greater Y_{ef} models as well as for the larger M ($= 2.0 M_\odot$) case (i.e., greater entropies, see Figs. 1-3). If we *assume* that the Y_e distribution by Buras et al. (2006) holds for the current models, the neutrino-driven winds may contribute the Galactic production of p -nuclei up to $A \sim 110$ (${}^{74}\text{Se}$, ${}^{78}\text{Kr}$, ${}^{84}\text{Sr}$, ${}^{92,94}\text{Mo}$, ${}^{96,98}\text{Ru}$, ${}^{102}\text{Pd}$, and ${}^{106,108}\text{Cd}$), which show considerable enhancements for $Y_{ef} \approx 0.50 - 0.56$. For the winds with $L_\nu = 8 \times 10^{51}\text{ ergs s}^{-1}$ (Figure 13, *middle panels*), it can be seen also that the heavier p -nuclei are highly enhanced as Y_{ef} increases. For $L_\nu = 2 \times 10^{51}\text{ ergs s}^{-1}$ (Figure 13, *bottom panels*), however, each p -process abundance reaches the maximum and decreases again as Y_{ef} increases. The reason is that the late winds in the current study cool down quickly below $T_9 \sim 2$ as can be seen in Figures 2 and 3. As a result, most of the proton-rich abundances produced during the rp -process phase ($T_9 \approx 3 - 2$, Fig. 7, *bottom left*) suffer neutron capture to *neutron-rich* isotopes (Fig. 7, *bottom right*), regardless of the large Y_{ef} as well as the high entropy.

For $Y_{ef} \approx 0.46 - 0.49$, some light p -nuclei (${}^{74}\text{Se}$, ${}^{78}\text{Kr}$, ${}^{84}\text{Sr}$, and ${}^{92}\text{Mo}$) are enhanced with interesting amounts (Fig. 13). Of particular importance is the production of ${}^{92}\text{Mo}$ as discussed in § 3.4. Hoffman et al. (1996) showed that a neutrino-driven wind having $Y_e \gtrsim 0.484$ cures the $N = 50$ overproduction (mostly ${}^{90}\text{Zr}$), which is replaced with the production of ${}^{92}\text{Mo}$. This strictly limited Y_e range is due to the competition between the production of ${}^{90}\text{Zr}$ (as the seed of ${}^{92}\text{Mo}$) in more neutron-rich winds and the concentration of protons (needed for the ${}^{92}\text{Mo}$ production) in

less neutron-rich winds. In the current study, the mass-averaged abundance of ^{92}Mo with respect to its solar value overcomes that of ^{90}Zr for wider range of Y_{ef} ($\approx 0.46 - 0.49$, Fig. 13, *top panels*). The reason is that the abundances are *mass averaged* over wide range of L_ν , not from a *single* wind trajectory. In particular, the earlier winds experience longer durations at $T_9 \approx 4 - 3$, at which the ^{92}Mo abundance is greatly enhanced (§ 3.4). In fact, for a specific wind, the enhancement of ^{92}Mo is limited to a smaller Y_{ef} range as can be seen in Figure 13 (*middle and bottom panels*). In addition, the position of Y_{ef} at which the ^{92}Mo abundance takes the maximum shifts toward 0.5 for lower L_ν (i.e., later winds). This is a consequence that the later winds cool down quickly below $T_9 \approx 4 - 3$, thus the proton richness (i.e., larger Y_e) is more important. In some later winds, relatively high entropies drive the material to form the QSE cluster that contains ^{90}Zr even with small neutron excess ($Y_{ef} \approx 0.49 - 0.50$), resulting in the enhancement of ^{92}Mo (Fig. 13, *middle right and bottom panels*).

The mass fractions of p -nuclei with respect to their solar values (Anders & Grevesse 1989) are also shown as functions of L_ν in Figure 14, for selected winds ($M = 1.4 M_\odot$; *left panels*, $M = 2.0 M_\odot$; *right panels*, $Y_{e0} = 0.48$; *top panels*, $Y_{e0} = 0.60$; *bottom panels*). For the winds with $Y_{e0} = 0.48$ ($Y_{ef} \approx 0.48$, as representative of slightly neutron-rich winds), ^{92}Mo is greatly enhanced at relatively early times ($L_\nu > 1 \times 10^{52} \text{ ergs s}^{-1}$, i.e., $t_{\text{pb}} < 0.8 \text{ s}$). This is due to the slow decrease of the temperature in the early winds at $T_9 \approx 4 - 3$, in which ^{92}Mo is most enhanced (§ 3.4). It should be cautioned that the steady wind approximation assumed in this study may not hold during the very early (*bubble*) phase ($t_{\text{pb}} < 0.5 \text{ s}$). However, it is likely that the material ejected as *bubbles* expand more slowly (e.g., Buras et al. 2006), and experiences longer time at $T_9 \approx 4 - 3$ in which ^{92}Mo might enhance to a similar (or more) degree. For the winds with $Y_{e0} = 0.60$ ($Y_{ef} \approx 0.54 - 0.56$, as representative of proton-rich winds), p -nuclei are enhanced at relatively later times ($L_\nu < 1 \times 10^{52} \text{ ergs s}^{-1}$, i.e., $t_{\text{pb}} > 0.8 \text{ s}$), where the steady wind approximation may hold (Figure 14, *bottom panels*). This is also consistent to the results by Pruet et al. (2005b), which showed no significant production of p -nuclei

in the bubbles. Note that no p -nuclei are produced in the very late winds ($L_\nu < 2 \times 10^{51} \text{ ergs s}^{-1}$, i.e., $t_{\text{pb}} > 4 \text{ s}$), in which the matter is assumed to be rather neutron rich (Fig. 4, *top panel*).

4.2. Mass- Y_e -averaged Yields

In reality, the neutrino-heated matter must have a certain distribution of Y_e when the multi-dimensional effects are taken into account. The problem is, of course, the unknown mechanism of core-collapse supernovae, which governs the hydrodynamic and thermodynamic histories of the neutrino-driven winds. Among a number of *artificially* induced explosion models, only the two-dimensional calculation with accurate neutrino transport by Buras et al. (2006) provides us a reliable Y_e distribution of the neutrino-processed material. The explosion in their simulation was obtained by omitting the velocity-dependent terms from the neutrino momentum equation. This led to the increase of the neutrino energy deposition in the heating region by a few 10%, which converted a failed model into an exploding one. The Y_e distribution $p(Y_e)$ of the neutrino-processed ejecta during the first 468 ms after core bounce for a $15 M_\odot$ progenitor star obtained by Buras et al. (2006) is overlaid in Figure 13. The histogram has the maximum at $Y_e \approx 0.5$ and dominates in the proton-rich side.

To test the contributions of the winds for $M = 1.4 M_\odot$ and $2.0 M_\odot$ models, the mass-averaged yields for each Y_{e0} model (Fig. 13, *top panels*) are further Y_e -averaged (~ 2000 winds in total for each M) with $p(Y_e)$, *assuming* this distribution to be representative of neutrino-driven winds. Needless to say, there is no guarantee that this distribution holds for the current wind models (at $t_{\text{pb}} = 4 \text{ s}$) for both $M = 1.4 M_\odot$ and $2.0 M_\odot$ cases. However, this is only the case obtained by a multi-dimensional hydrodynamic calculation with *accurate* neutrino transport that is essential to predict the Y_e distribution of the neutrino-heated ejecta. It may be, therefore, interesting to see the possible contributions to the Galactic chemical evolution with this $p(Y_e)$, keeping in mind that a more consistent estimation of $p(Y_e)$ will be needed in the future study.

The resulting abundances with respect to their solar values are shown in Figure 15 for $M = 1.4 M_\odot$ (*top panel*) and $2.0 M_\odot$ (*bottom panel*)

models as functions of mass number. The abundances smaller than $X_{\text{ej}}/X_{\odot} < 100$ are omitted here. The even- Z and odd- Z isotopes for a given element are denoted by circles and triangles, respectively, which are connected by lines. The p -nuclei are marked with filled symbols. The dotted horizontal lines indicate a “normalization band” (Woosley et al. 1994) between the largest production factor (^{100}Mo for $M = 1.4 M_{\odot}$ and ^{92}Mo for $M = 2.0 M_{\odot}$) and that by a factor of ten less than that, along with the median value (*dashed line*). This band is taken to be representative of the uncertainty in the nuclear data involved.

When compared with the results in which the mass average is only for $L_{\nu} \geq 2 \times 10^{51} \text{ ergs s}^{-1}$ (Fig. 16, *top panels*), it is clear that the later winds for $L_{\nu} < 2 \times 10^{51} \text{ ergs s}^{-1}$ contribute to only the r -nuclei with $A > 90$ but to p -nuclei. Figure 15 implies that there exists a correlation between the production of p -nuclei and r -nuclei. That is, the higher entropy model ($M = 2.0 M_{\odot}$) produces heavier p -nuclei (up $A \sim 110$) and r -nuclei (up to $A \sim 190$) in a *single* event. This might be true, since both the rp -process and r -process favor the high entropy conditions. It would be premature to conclude that, however, when considering the highly uncertain late-time evolution of neutrino-driven winds. It is interesting to note that no overproduction of the $N = 50$ ($A \approx 90$) nuclei (Woosley et al. 1994; Wanajo et al. 2001) appears owing to the neutron deficiency in the ejecta (Hoffman et al. 1996; Wanajo & Ishimaru 2006).

Hereafter, only the winds for $L_{\nu} \geq 2 \times 10^{51} \text{ ergs s}^{-1}$ ($t_{\text{pb}} \leq 4 \text{ s}$) are considered, in which the p -nuclei are produced. Noted that the production of ^{64}Zn that is the dominant stable zinc isotope (but its origin is unknown, see Hoffman et al. 1996; Umeda & Nomoto 2002; Pruet et al. 2005a; Fröhlich et al. 2006) is about 10 times smaller the lower normalization band, much smaller than expected in Hoffman et al. (1996, see also Fig. 13). The contributions to the production of ^{45}Sc and ^{49}Ti are not important either, which are suggested to be produced in the earlier ejecta (Pruet et al. 2005a; Fröhlich et al. 2006).

Figure 16 compares the results with (*top panels*) and without (*bottom panels*) neutrino reactions (eqs. [1]-[6]) for the $M = 1.4 M_{\odot}$ (*left panels*) and $2.0 M_{\odot}$ (*right panels*) models. As can be seen, the production of almost all ^{92}Mo and

some portions of ^{74}Se , ^{78}Kr , and ^{84}Sr are not due to the effect of neutrino reactions. This can be also seen in Figure 17, which compares the results from only neutron-rich (*top panels*) or proton-rich (*bottom panels*) winds for the $M = 1.4 M_{\odot}$ (*left panels*) and $2.0 M_{\odot}$ (*right panels*) models. ^{92}Mo is highly overproduced in the mass average of neutron-rich winds, which is, on the contrary, somewhat underproduced in the proton-rich winds compared to other light p -nuclei (e.g., ^{74}Se , ^{78}Kr , ^{84}Sr , ^{94}Mo , and $^{96,98}\text{Ru}$). Hence, the bulk of ^{92}Mo originates from the slightly neutron-rich winds ($Y_{\text{ef}} \approx 0.46 - 0.50$), while other p -nuclei from mainly proton-rich winds.

When we look at the top panels of Figure 16 again, the p -nuclei up to ^{92}Mo and ^{108}Cd for $M = 1.4 M_{\odot}$ and $2.0 M_{\odot}$ models, respectively, fall within the normalization band, which are regarded to be the dominant species produced by each event. It is interesting to note that the contributions to ^{94}Mo , $^{96,98}\text{Ru}$, and ^{102}Pd for $M = 1.4 M_{\odot}$ and $^{112,114,115}\text{Sn}$, and ^{113}In for $M = 2.0 M_{\odot}$ are marginal. The ejected masses by winds during the first 20 s are $3.0 \times 10^{-3} M_{\odot}$ and $1.2 \times 10^{-3} M_{\odot}$ for the current $M = 1.4 M_{\odot}$ and $2.0 M_{\odot}$ models, respectively. Given that the progenitor mass for each case to be, e.g., $15 M_{\odot}$ and $30 M_{\odot}$, respectively, the overproduction factor is expressed as $\sim 10^{-4} (X_{\text{ej}}/X_{\odot})$. The requisite overproduction factor for the nucleosynthetic event to be the major source in the solar system is ~ 10 (Woosley et al. 1994), assuming that *all* the core-collapse supernovae produce the same amount of the isotope. The overproduction factors of $\sim 10 - 100$ (Fig. 16, *top panels* or Fig. 15) for the current models imply that the neutrino-driven winds can be potentially the major astrophysical site of these light p -nuclei.

5. Summary and Conclusions

In this study, the neutrino-induced rp -process in neutrino-driven winds has been investigated. The thermodynamic histories of winds were obtained from the semi-analytic models of the neutrino-driven winds that had been developed for the r -process study in previous works. The subsonic wind solutions with the nearly maximum mass ejection rates were taken in this study, for various neutrino luminosities ($40 - 0.5 \times 10^{51} \text{ ergs s}^{-1}$) with the proto-neutron star

masses of $1.4 M_{\odot}$ and $2.0 M_{\odot}$. The latter ($2.0 M_{\odot}$) was regarded as the test case of higher entropy winds (about a factor of two), which might be expected in more realistic hydrodynamic simulations of core-collapse supernovae. The nucleosynthesis calculations were performed for the wide range of the initial electron fractions ($0.45 \leq Y_{e0} \leq 0.65$) including rather proton-rich compositions, motivated by recent hydrodynamic results. The main results of this study can be summarized as follows:

1. In the proton-rich winds, the proton capture can proceed beyond the iron-group nuclei, by bypassing the known β^+ -waiting point nuclei (e.g., ^{64}Ge) via (n, p) reactions, as also suggested by recent works (Fröhlich et al. 2005, 2006; Pruet et al. 2005b; Wanajo 2005). These neutrons are continuously supplied from the anti-electron neutrino capture on abundant free protons.

2. The neutrino-induced rp -process leads to the production of some light p -nuclei, even with moderate entropy ($\sim 50 N_A k$) that can be found in the early winds ($t_{\text{pb}} \sim 1$ s) from the neutron star with $1.4 M_{\odot}$. The production of p -nuclei is, however, highly dependent on the entropy in the wind, which affects the proton-to-seed abundance ratio Y_p/Y_h at the beginning of the rp -process. In the high entropy winds ($\sim 100 N_A k$) with $M = 2.0 M_{\odot}$, the nuclear flow proceeds to $Z \approx 50$, resulting in the production of p -nuclei up to $A \sim 130$.

3. The production of p -nuclei is also highly sensitive to the proton richness of the wind material. In the slightly proton-rich winds ($Y_e \sim 0.50 - 0.52$), only the lightest p -nuclei (^{74}Se , ^{78}Kr , and ^{84}Sr) are produced. The higher p -nuclei up to $A \sim 130$ are synthesized with interesting amounts as Y_e rises to ~ 0.56 .

4. The termination of the rp -process is due to the increasing Coulomb barrier for the heaviest nuclei in the nuclear flow, *not* due to the exhaustion of free protons. The decrease of the temperature below $\sim 2 \times 10^9$ K owing to the expansion of the ejecta is also a cause of the termination. The supply of neutrons by the neutrino capture on protons is sufficient throughout the rp -process phase. Hence the dilution of the neutrino flux by the expansion of matter is not the principal reason for the termination of the rp -process in the current wind models.

5. Few p -nuclei beyond $A \sim 130$ are produced by the neutrino-induced rp -process, owing to the increasing Coulomb barrier for heavier nuclei. The high entropy ($\sim 200 N_A k$) or highly proton-rich ($Y_e \sim 0.6$) wind results in driving the nuclear abundances to the β -stability or even the neutron-rich region, when the temperature drops below $T_9 \sim 2$. In this case, a variety of neutron-rich isotopes, which are generally assigned to s -nuclei or r -nuclei, are synthesized even in the proton-rich compositions.

6. ^{92}Mo is produced with interesting amounts in the slightly neutron-rich winds ($Y_e \sim 0.46 - 0.49$), much more than in the proton-rich winds. This is due to the proton capture reactions at $T \sim 4 - 3 \times 10^9$ K, which carry a portion of the nuclear abundances from the abundant ^{90}Zr to ^{92}Mo . The amount of the produced ^{92}Mo is, however, highly dependent on the thermodynamic history of the wind.

7. The neutrino-driven winds can be the origin of some light p -nuclei, at least of ^{74}Se , ^{78}Kr , ^{84}Sr , and ^{92}Mo , and likely of ^{94}Mo , $^{96,98}\text{Ru}$, ^{102}Pd , and $^{106,108}\text{Cd}$, supplemented by the production of ^{92}Mo in the slightly neutron-rich compositions. In particular, this can be the unique astrophysical site responsible for the production of the proton-rich Mo and Ru isotopes. The heavier p -nuclei ($A > 110$) may have another origin, most likely the O/Ne layers in core-collapse supernovae (Prantzos et al. 1990; Rayet et al. 1995). Note that the p -nuclei synthesized in neutrino-driven winds are regarded as *primary*. This is contrast to those produced in the O/Ne layers, which need the s -process seed abundances and thus regarded as *secondary*.

Note that the neutrino-induced rp -process in the current study may not contribute to the production of any *elements*, since the fraction of p -process isotopes for a given element is generally an order of one percent. Therefore, it would be challenging to confirm the occurrence of the neutrino-induced rp -process by spectroscopic studies of extremely metal-poor stars, which are expected to preserve the nucleosynthetic signature from a single (or a few) supernova (e.g., Ishimaru & Wanajo 1999; Wanajo & Ishimaru 2006). Analysis of the isotope anomalies in some elements found in primitive meteorites (e.g., Arnould & Goriely 2003) might provide us some clues.

At the end of this investigation, it should be cautioned that the nucleosynthesis calculations in the current study are based on a schematic formulation of neutrino-driven winds, which must be in fact closely related to the unknown mechanism of core-collapse supernovae. In addition, the estimation of the p -nuclei production in each event (i.e., the core-collapse supernova that leaves the proto-neutron star with $1.4 M_{\odot}$ or $2.0 M_{\odot}$) was based on the Y_e distribution during the *bubble* (not wind) phase, obtained from one specific hydrodynamic simulation (Buras et al. 2006). Therefore, the current results should *not* be regarded as the quantitative (but qualitative) predictions that is to be used for the Galactic chemical evolution study.

Nevertheless, the current study provides us some notable implications. First, it is likely that the neutrino-induced rp -process takes place in *all* core-collapse supernovae to some extent, even with a moderate entropy. In this sense, other astrophysical sites than standard core-collapse events, e.g., collapsar jets or disk winds formed around a black hole, which are associated to gamma-ray bursts, can be the astrophysical site for the neutrino-induced rp -process. Second, details of the nucleosynthesis process are presented for selected winds, which will be useful for the future experimental studies of proton-rich nuclei far from the β -stability. In particular, core-collapse supernovae no doubt eject the nucleosynthetic products that contribute to the Galactic chemical evolution of heavy nuclei. This is in contrast to X-ray bursts, which is unlikely to contribute the Galactic chemical evolution. Therefore the experimental estimations can be easily tested by comparing the nucleosynthesis calculations to, e.g., the solar compositions. Third, the systematic calculations for the wide (but reasonable) ranges of the neutrino luminosities and the electron fractions enable us to make a meaningful comparison with the solar abundances. This may serve unique constraints to the fluid dynamics of the early supernova ejecta, if we *assume* that the light p -nuclei originate from core-collapse supernovae. I hope the current results provide some fresh insights to the future modeling of core-collapse supernovae as the astrophysical site of the neutrino-induced rp -process.

This work was supported in part by a Grant-in-

Aid for Japan-France Integrated Action Program (SAKURA) from the Japan Society for the Promotion of Science, and Scientific Research (17740108) from the Ministry of Education, Culture, Sports, Science, and Technology of Japan.

REFERENCES

- Aikawa, M., Arnould, M., Goriely, S., Jorissen, A., & Takahashi, K. 2005, *A&A*, 441, 1195
- Anders, E., & Grevesse, N. 1989, *Geochim. Cosmochim. Acta*, 53, 197
- Arnould, M. & Goriely, S. 2003, *Phys. Rep.*, 384, 1
- Audi, G., Wapstra, A. H., & Thibault, C. 2003, *Nucl. Phys. A*, 729, 337
- Buras, R., Rampp, M., Janka, H. -Th., & Kifonidis, K. 2005, *A&A*, 447, 1049
- Burrows, A., Livne, E., Dessart, L., Ott, C. D., & Murphy, J. 2005, *ApJ*, in press (astro-ph/0510687)
- Cardall, C. Y. & Fuller, G. M. 1997, *ApJ*, 486, L111
- Fuller, G. M., Fowler, W. A., & Newman, M. J. 1982, *ApJS*, 48, 279
- Fröhlich, C., et al. 2006, *ApJ*, 637, 415
- Fröhlich, C., et al. 2005, *Phys. Rev. Lett.*, submitted (astro-ph/0511376)
- Goriely, S., Samyn, M., Pearson, J. M., & Onsi, M. 2005, *Nucl. Phys. A*, 750, 425
- Hoffman, R. D., Woosley, S. E., Fuller, G. M., & Meyer, B. S. 1996, *ApJ*, 460, 478
- Ishimaru, Y. & Wanajo, S. 1999, *ApJ*, 511, L33
- Koike, O., Hashimoto, M., Arai, K., & Wanajo, S. 1999, *A&A*, 342, 464
- Kitaura, F. S., Janka, H. -Th., & Hillebrandt, W. 2005, *A&A*, submitted (astro-ph/0512065)
- Langanke, K. & Martinez-Pinedo, G. 2001, *At. Data Nucl. Data Tables*, 79, 1

- Liebrandt, M., Mezzacappa, A., Messer, O. E. B., Martinez-Pinedo, G., Hix, W. R., & Thielemann, F. -K. 2003, Nucl. Phys. A, 719, 144
- McLaughlin, G. C., Fuller, G. M., & Wilson, J. R. 1996, ApJ, 472, 440
- Meyer, B. S. 1995, ApJ, 449, L55
- Meyer, B. S., McLaughlin, G. C., & Fuller G. M. 1998, Phys. Rev. C, 58, 3696
- Otsuki, K., Tagoshi, H., Kajino, T., & Wanajo, S. 2000, ApJ, 533, 424
- Pruet, J., Woosley, S. E., Buras, R., & Janka, H. -Th. 2005, ApJ, 623, 325
- Pruet, J., Hoffman, R. D., Woosley, S. E., Buras, R., & Janka, H. -Th. 2005, ApJ, submitted (astro-ph/0511194)
- Prantzos, N., Hashimoto, M., Rayet, M., & Arnould, M. 1990, A&A, 238, 455
- Qian, Y. -Z. & Woosley, S. E. 1996, ApJ, 471, 331
- Qian, Y. -Z., Haxton, W. C., Langanke, K., & Vogel, P. 1997, Phys. Rev. C, 55, 1532
- Rayet, M., Arnould, M., Hashimoto, M., Prantzos, N., & Nomoto, K. 1995, A&A, 298, 517
- Schatz, H, et al. 1998, Phys. Rep., 294, 167
- Suzuki, T. K. & Nagataki, S. 2005, ApJ, 628, 914
- Tachibana, T., Yamada, M., & Yoshida, Y. 1990, Progr. Theor. Phys., 84, 641
- Thompson, T. A., Burrows, A., & Meyer, B. S. 2001, ApJ, 562, 887
- Thompson, T. A. 2003, ApJ, 585, L33
- Umeda, H. & Nomoto, K. 2002, ApJ, 565, 385
- Wallace, R. K. & Woosley, S. E. 1981, ApJS, 45, 389
- Wanajo, S., Kajino, T., Mathews, G. J., & Otsuki, K. 2001, ApJ, 554, 578
- Wanajo, S., Itoh, N., Ishimaru, Y., Nozawa, S., & Beers, T. C. 2002, ApJ, 577, 853
- Wanajo, S., Goriely, S., Samyn, M., & Itoh, N. 2004, ApJ, 606, 1057
- Wanajo, S. 2005, in Proc. Origin of Matter and Evolution of Galaxies (8-11 November 2005, Tokyo), ed. S. Kubono, in press
- Wanajo, S. & Ishimaru, I. 2006, Nucl. Phys. A, in press (doi:10.1016/j.nuclphysa.2005.10.012)
- Woosley, S. E., Hartmann, D. H., Hoffman, R. D., & Haxton, W. C. 1990, ApJ, 356, 272
- Woosley, S. E., Wilson, J. R., Mathews, G. J., Hoffman, R. D., & Meyer, B. S. 1994, ApJ, 433, 229
- Woosley, S. E., et al. 2004, ApJS, 151, 75

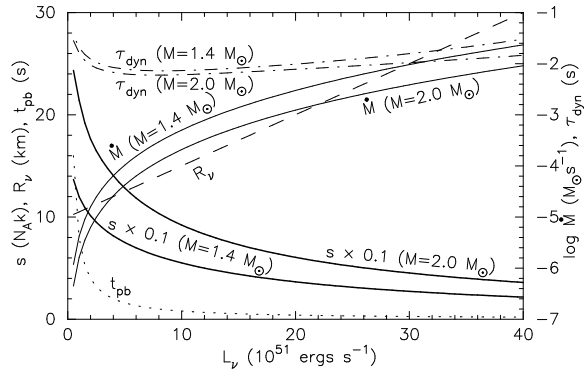


Fig. 1.— Model parameters (R_ν, t_{pb}, \dot{M}) of the current neutrino-driven winds are shown as functions of L_ν . Also denoted are the obtained entropies (s) and dynamic timescales (τ_{dyn}) for $1.4 M_\odot$ and $2.0 M_\odot$ cases.

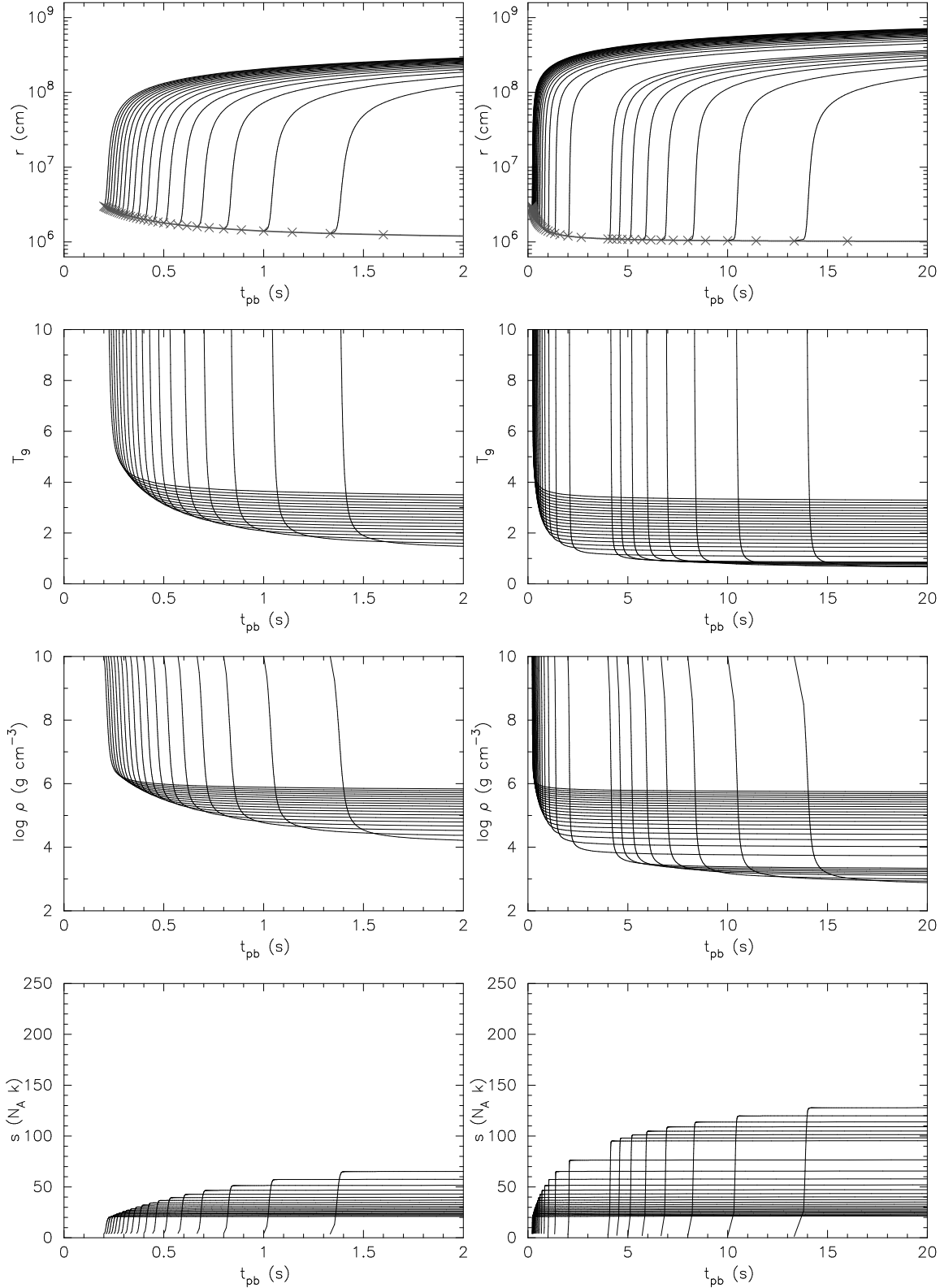


Fig. 2.— Time variations of radius, temperature, density, and entropy for selected (odd-numbered) wind trajectories with the $M = 1.4 M_{\odot}$ model ($t_{\text{pb}} \leq 2\text{ s}$ and $t_{\text{pb}} \leq 20\text{ s}$ for *left* and *right panels*, respectively). The evolution of the neutrino sphere is denoted by the grey lines along with the starting point for each wind (crosses) in top panels.

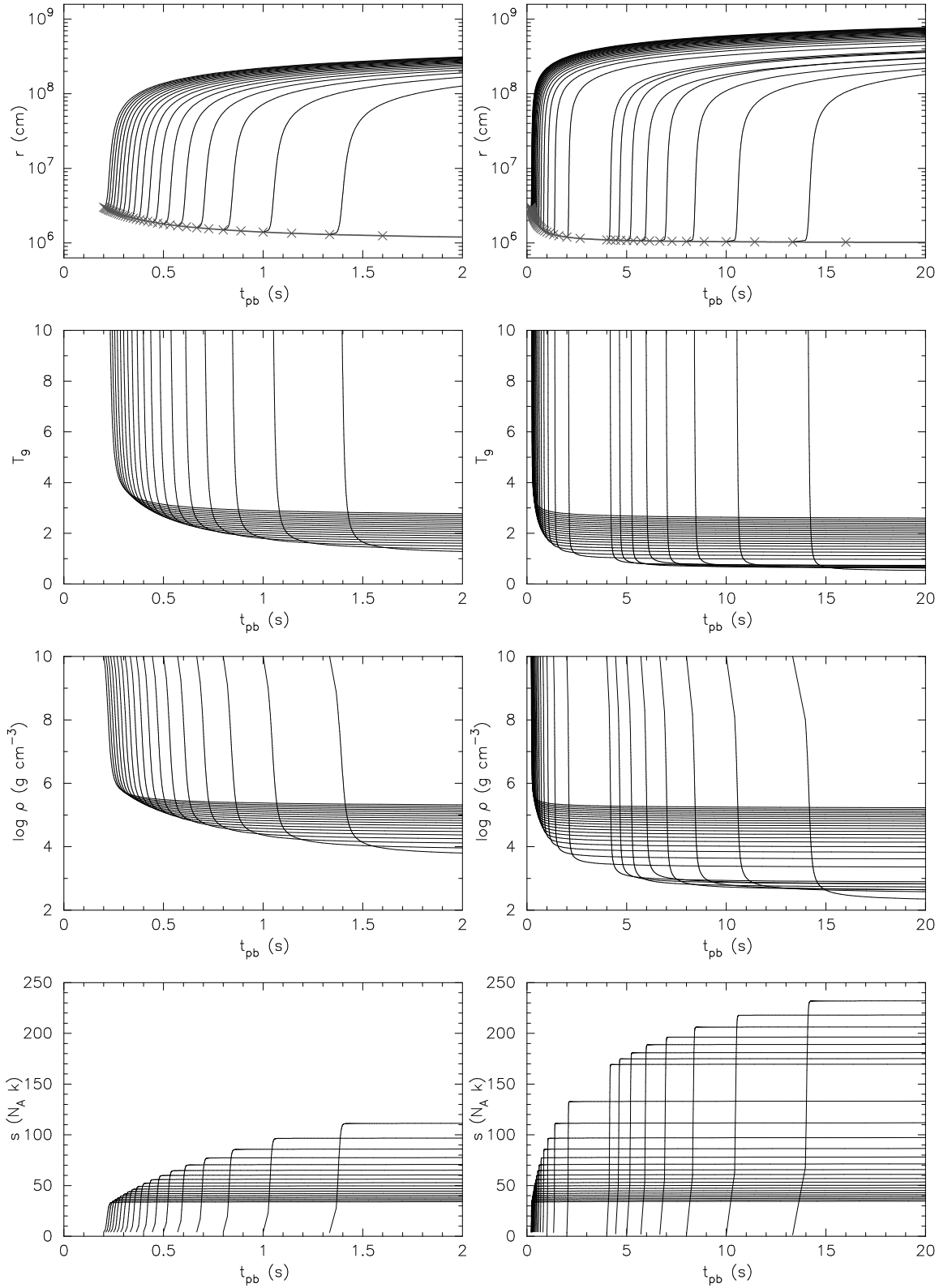


Fig. 3.— Same as Figure 2, but for the $M = 2.0 M_{\odot}$ model.

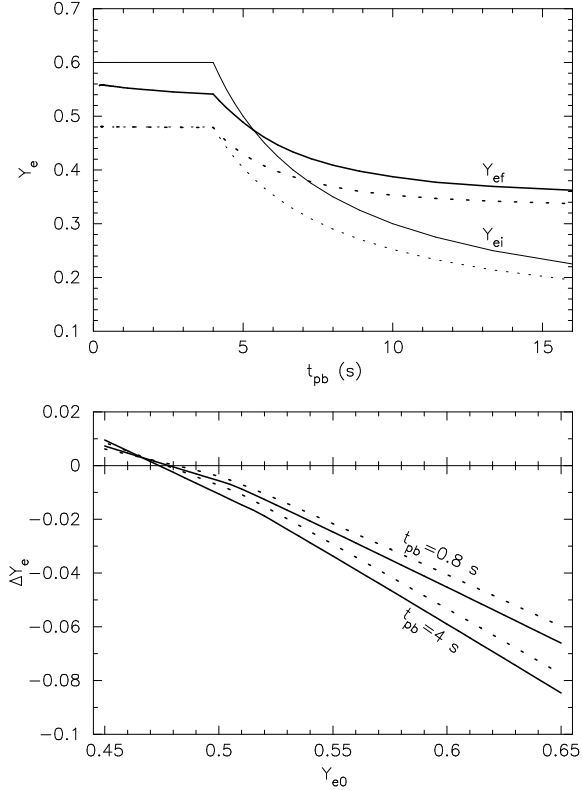


Fig. 4.— *Top*: Y_e at $T_9 = 9$ (Y_{ei} , *thin lines*) and at $T_9 = 3$ (Y_{ef} , *thick lines*) as functions of t_{pb} . The solid and dotted lines denote the results for $M = 2.0 M_\odot$ with $Y_{e0} = 0.60$ and $M = 1.4 M_\odot$ with $Y_{e0} = 0.48$, respectively. *Bottom*: Differences of Y_e ($\Delta Y_e \equiv Y_{ei} - Y_{ef}$) at $t_{pb} = 0.8$ s and 4.0 s as functions of Y_{e0} , for $M = 1.4 M_\odot$ (*dotted lines*) and $2.0 M_\odot$ (*solid lines*).

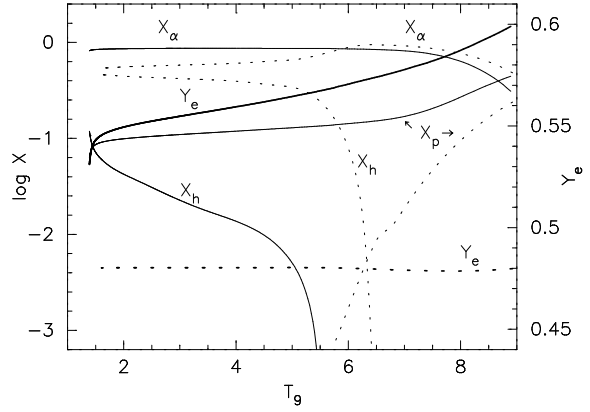


Fig. 5.— Variations of Y_e (*thick lines*) and the mass fractions (*thin lines*) of neutrons (X_n), protons (X_p), α particles (X_α), and heavy nuclei (X_h) as functions of T_9 . The solid and dotted lines denote the results for the wind trajectories W201060 and W141048 (see the text and footnote 1), respectively.

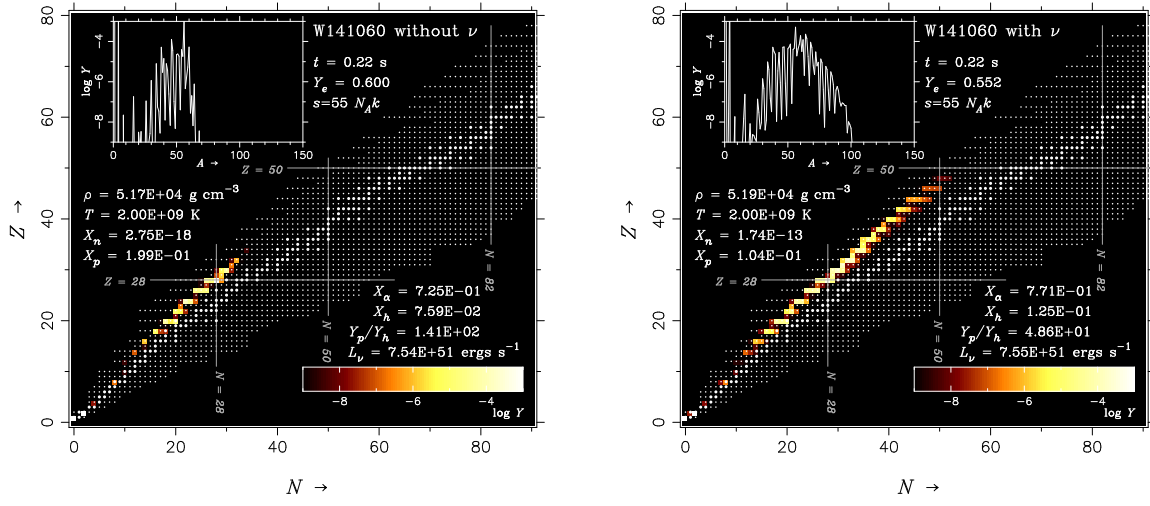


Fig. 6.— Snapshots of the nucleosynthesis calculations at $t = 0.22$ s for the wind trajectory of W141060, in which the neutrino-induced reactions (eqs. [1]-[6]) are turned off (*left panel*) and on (*right panel*). The temperature decreases to $T_9 \approx 2$ at this time. The abundances are color coded in the nuclide chart. The nuclei included in the reaction network are denoted by dots, with the stable isotopes represented by large dots. The abundance curve as a function of mass number is shown in the upper left for each panel.

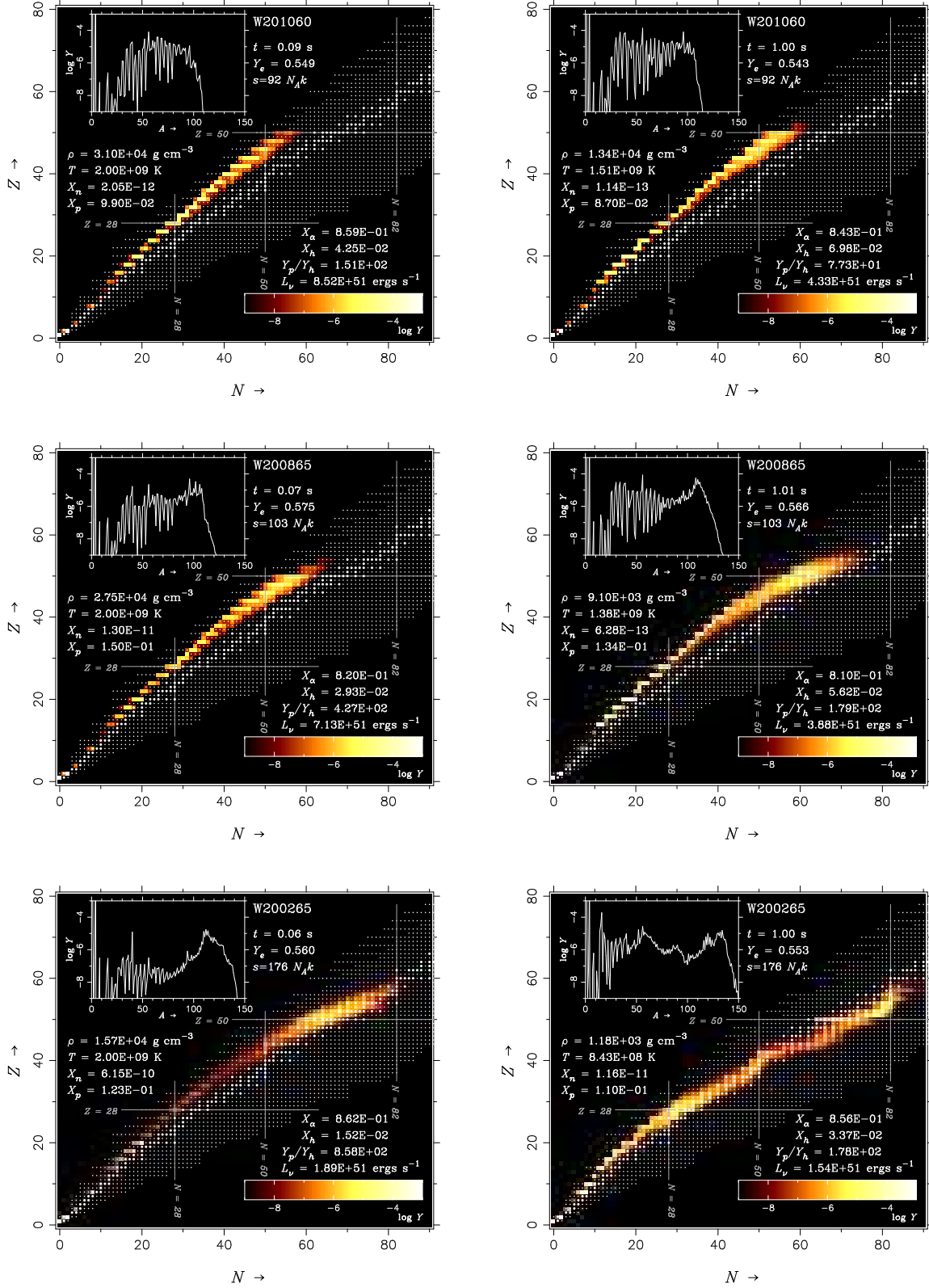


Fig. 7.— Same as Figure 6, but for the wind trajectories of W201060 (top), W200865 (middle), and W200265 (bottom). Left and right panels are the snapshots at $T_9 \approx 2.0$ and $t_{pb} \approx 1.0$ s, respectively. Neutrino-induced reactions (eqs. [1]-[6]) are included for all cases.

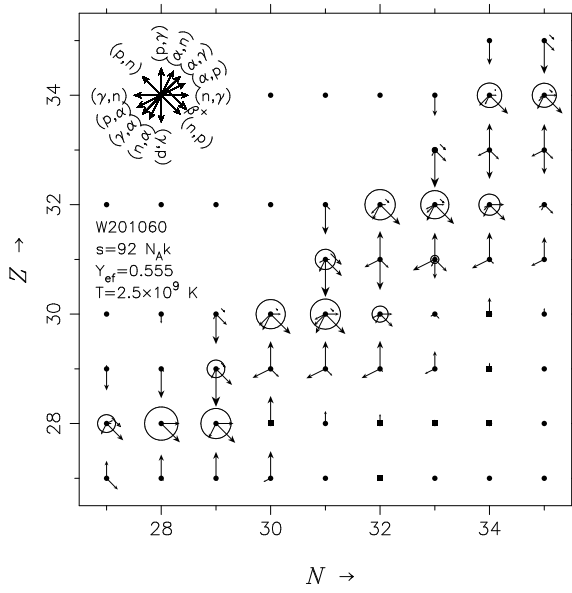


Fig. 8.— Nuclear flows defined by equation (9) (*arrows*) and the abundances (*circles*) in logarithmic scale for the wind trajectory of W201060 at $T_9 = 2.5$, for those greater than 10^{-5} . The flows by β^+ -decays are denoted by off-centered arrows. The nuclei included in the reaction network are denoted by dots, with the stable isotopes represented by squares.

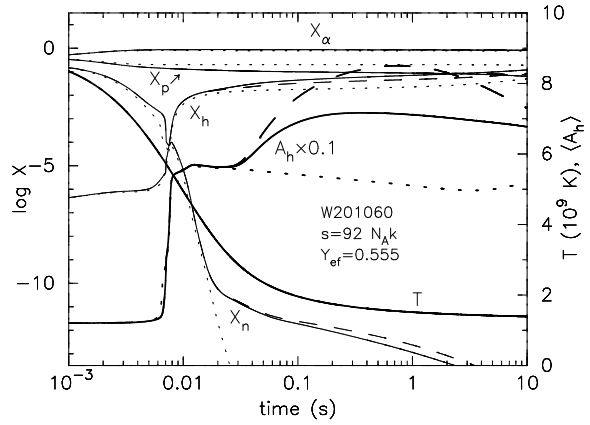


Fig. 9.— Time variations of the mass fractions (*thin lines*) of neutrons X_n , protons X_p , α particles X_α , and heavy nuclei X_h for the wind trajectory W201060. The solid, dashed, and dotted lines denote the results with all neutrino-induced reactions (eqs. [1]-[6]), neutrino capture on free nucleons only (eqs. [1] and [2]), and no neutrino-induced reactions, respectively. Also shown are the average mass number of heavy nuclei A_h and the temperature (*thick lines*).

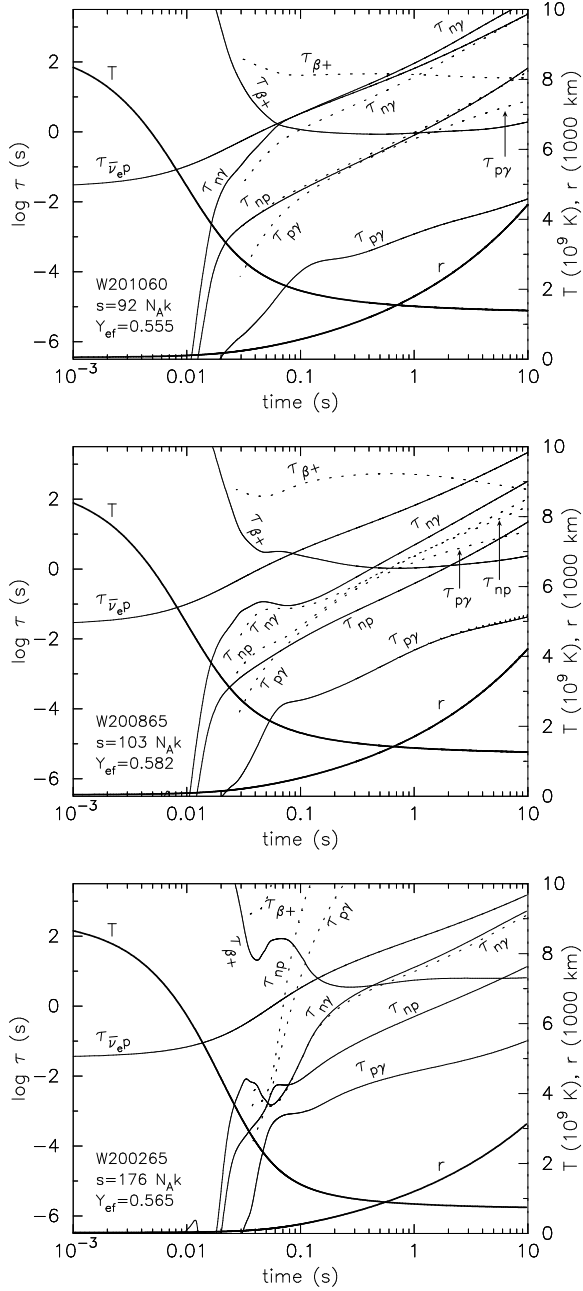


Fig. 10.— Time variations of the mean lifetimes for β^+ -decay, (n, γ) , (p, γ) , and (n, p) reactions, and neutrino capture on protons for the wind trajectories of W201060 (*top*), W200865 (*middle*), and W200265 (*bottom*), defined by equations (12)-(16). The solid and dotted lines denote the lifetimes for $Z \geq 2$ and $Z \geq 48$ nuclei, respectively. For the latter, the values for only $T_9 < 3$ are shown, in which these nuclei are synthesized by the rp -process. Also shown are the temperature and the distance from the center of the neutron star (*thick lines*).

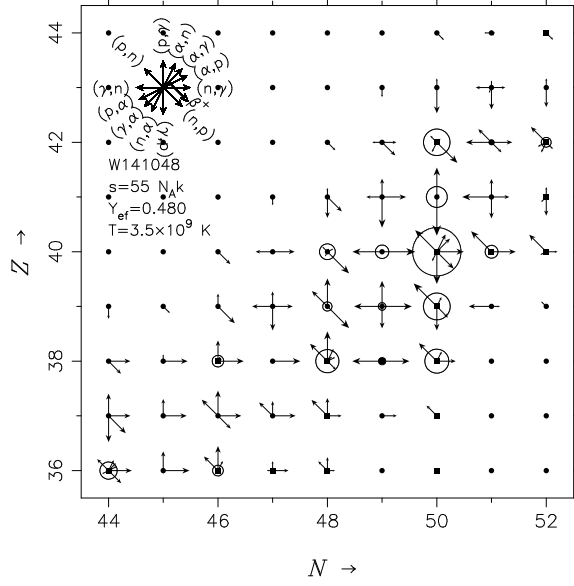


Fig. 11.— Same as Figure 8, but for the wind trajectory of W141048.

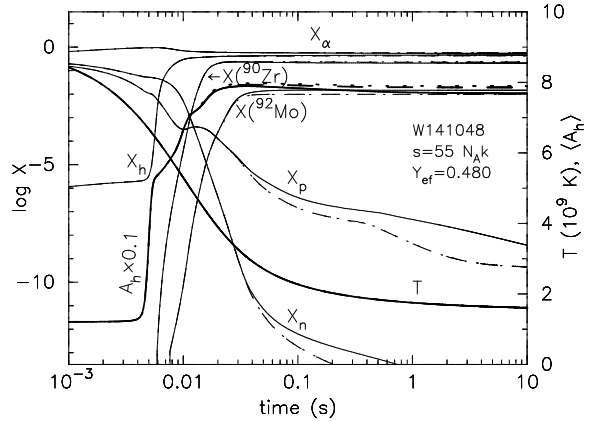


Fig. 12.— Same as Figure 9, but for the wind trajectory of W141048. The mass fractions of ^{90}Zr and ^{92}Mo are also plotted.

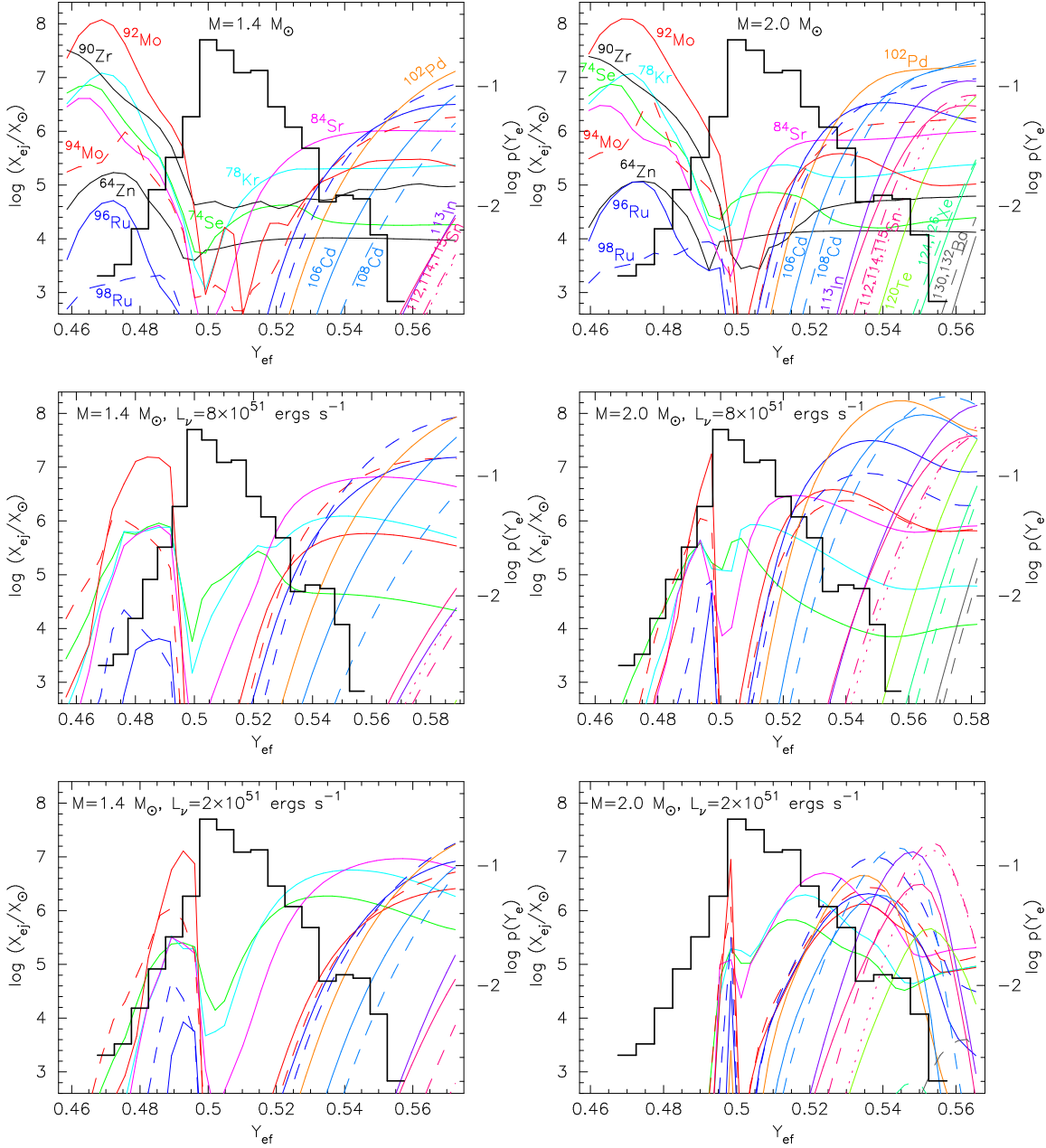


Fig. 13.— Mass fractions X_{ej} of p -nuclei with respect to their solar values (X_{\odot} , Anders & Grevesse 1989) as functions of Y_{ef} for $M = 1.4 M_{\odot}$ (left) and $2.0 M_{\odot}$ (right) models. Top panels show the mass-averaged results (see the text), where Y_{ef} is taken to be that at $t_{pb} = 4$ s ($L_{\nu} = 2 \times 10^{51}$ ergs s^{-1}). The mass fractions of ^{64}Zn and ^{90}Zr are also plotted for comparison purposes. Middle and bottom panels show the results for the winds with $L_{\nu} = 8 \times 10^{51}$ ergs s^{-1} and 2×10^{51} ergs s^{-1} , respectively. The histogram is the asymptotic Y_e distribution $p(Y_e)$ of the neutrino-processed ejecta during the first 468 ms after core bounce for a $15 M_{\odot}$ progenitor star taken from Buras et al. (2006).

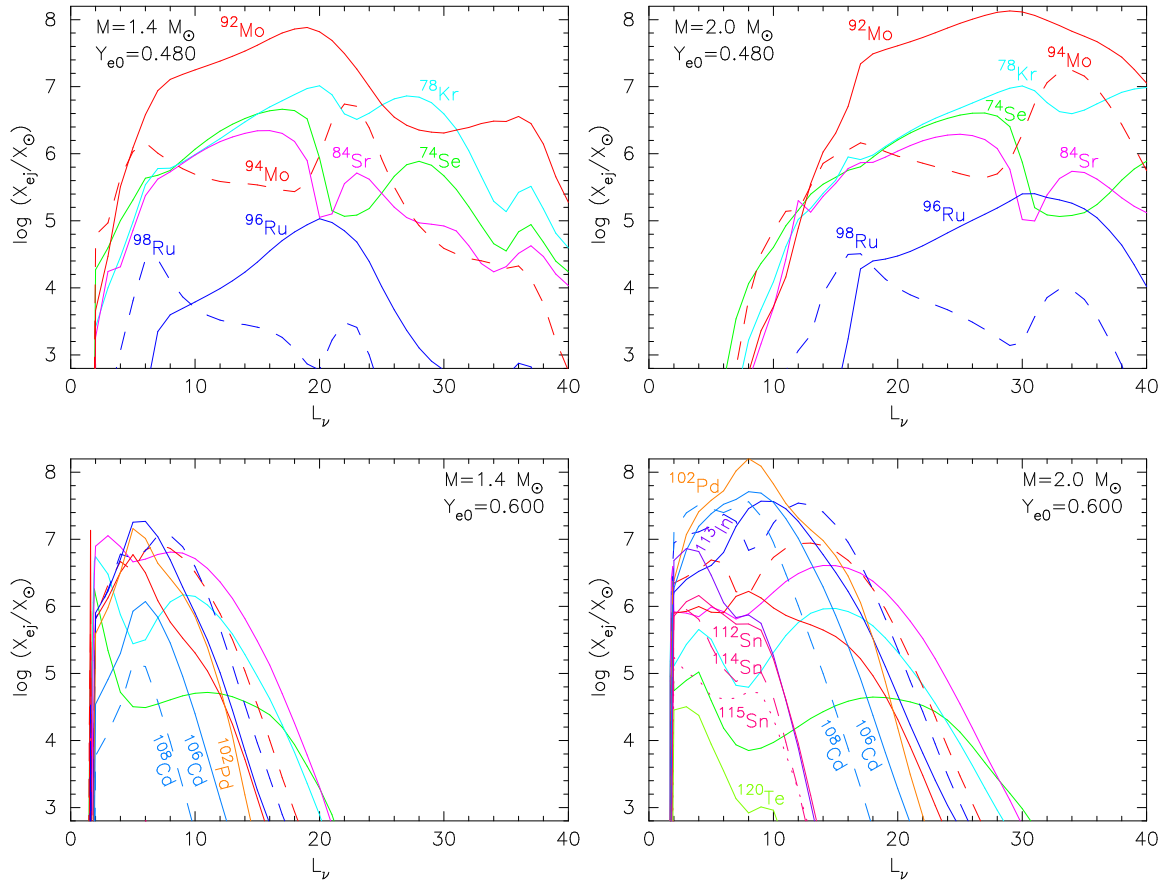


Fig. 14.— Mass fractions of p -nuclei with respect to their solar values (Anders & Grevesse 1989) as functions of L_ν , for the selected cases ($M = 1.4 M_\odot$; *left*, $M = 2.0 M_\odot$; *right*, $Y_{e0} = 0.48$; *top*, $Y_{e0} = 0.60$; *bottom*).

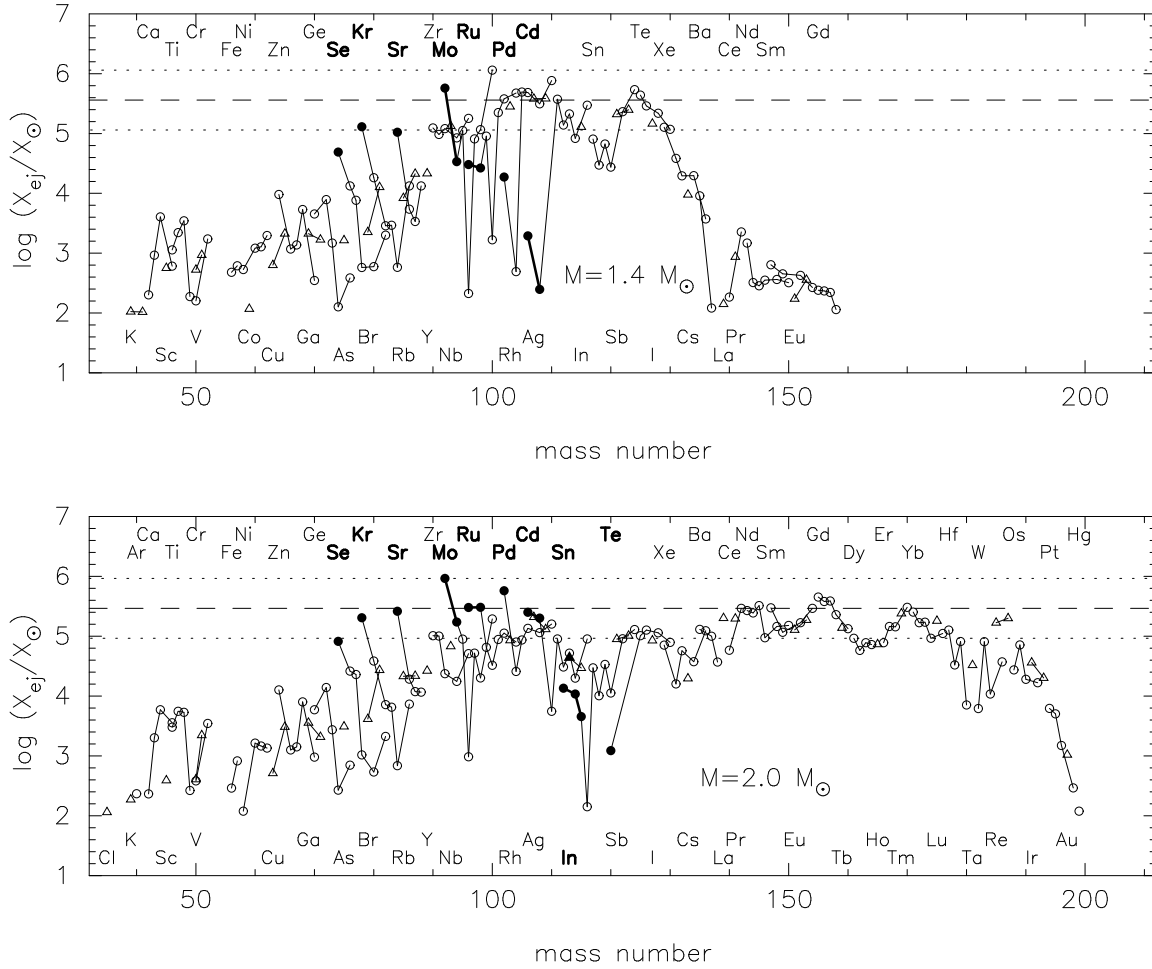


Fig. 15.— Mass- Y_e -averaged abundances with respect to their solar values (Anders & Grevesse 1989) for $M = 1.4 M_{\odot}$ (top) and $2.0 M_{\odot}$ (bottom) models as functions of mass number (see the text). The abundances smaller than $X_{ej}/X_{\odot} < 100$ is omitted here. The isotopes (after decay) are denoted by open circles (even- Z) and triangles (odd- Z). The p -nuclei are denoted with filled symbols. The solid lines connect isotopes of a given element.

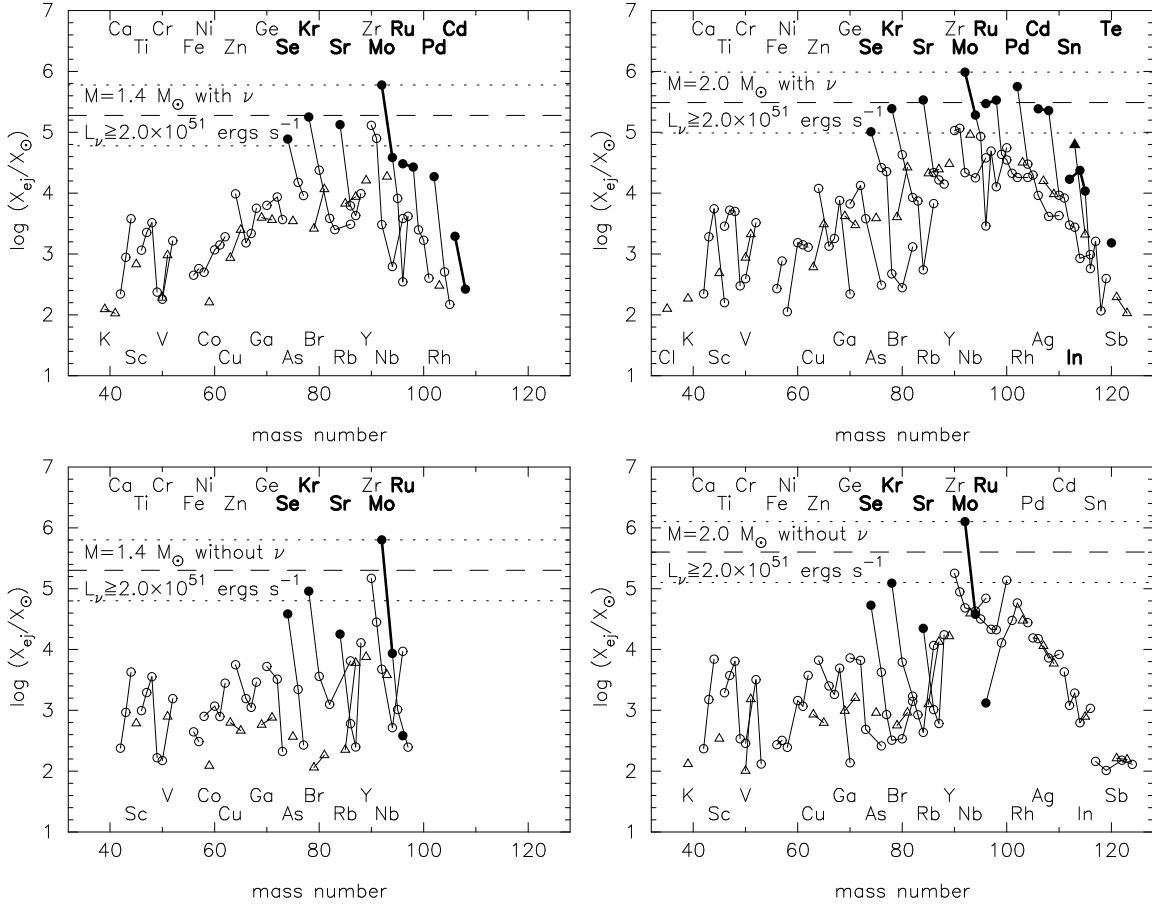


Fig. 16.— Same as Figure 15, but for $L_\nu \geq 2 \times 10^{51} \text{ ergs s}^{-1}$ ($t_{\text{pb}} \leq 4 \text{ s}$). Top and bottom panels show the results with and without neutrino-induced reactions (eqs. [1]-[6]), respectively.

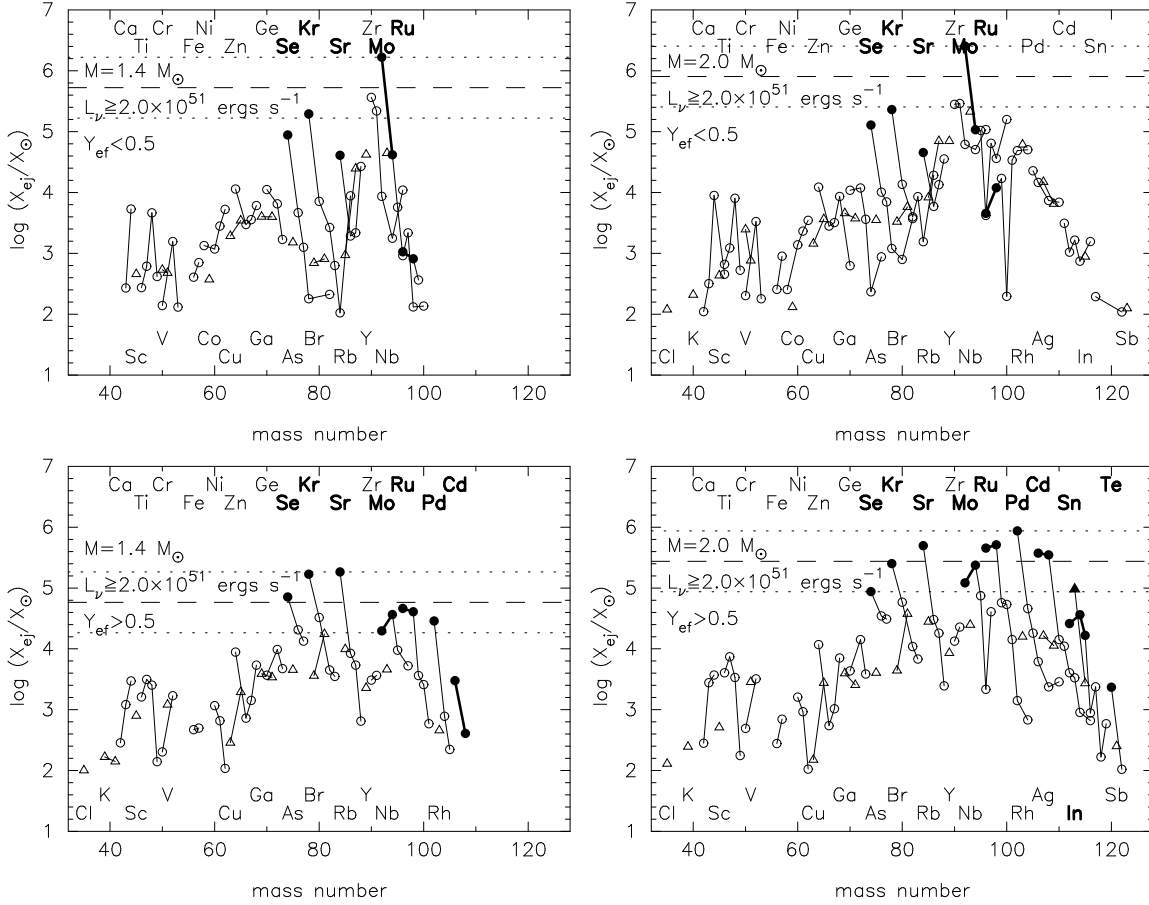


Fig. 17.— Same as Figure 15, but for $L_{\nu} \geq 2 \times 10^{51} \text{ ergs s}^{-1}$ ($t_{pb} \leq 4 \text{ s}$). Top and bottom panels show the results for the neutron-rich ($Y_{ef} < 0.5$) and proton-rich ($Y_{ef} > 0.5$) winds, respectively.